The Proceedings of the International Conference on Creationism

Volume 8 Article 12

2018

Finite element analysis of large body deformation induced by a catastrophic near impact event

DOI: https://doi.org/10.15385/jpicc.2018.8.1.9

Denver W. Seely
Mississippi State University

Andrew Bowman
Mississippi State University

Heechen Cho
Mississippi State University

Mark Horstemeyer
Mississippi State University

Recommended Citation

Seely, D., A.L. Bowman, N. Cho, and M.F. Horstemeyer. 2018. Finite element analysis of large body deformation induced by a catastrophic near impact event. 2018. In Proceedings of the Eighth International Conference on Creationism, ed. J.H. Whitmore, pp. 52–70. Pittsburgh, Pennsylvania: Creation Science Fellowship.

Seely, D., A.L. Bowman, N. Cho, and M.F. Horstemeyer. 2018. Finite element analysis of large body deformation induced by a catastrophic near impact event. 2018. In *Proceedings of the Eighth International Conference on Creationism*, ed. J.H. Whitmore, pp. 52–70. Pittsburgh, Pennsylvania: Creation Science Fellowship.

FINITE ELEMENT ANALYSIS OF LARGE BODY DEFORMATION INDUCED BY A CATASTROPHIC NEAR IMPACT EVENT

Denver Seely, Center for Advanced Vehicular Systems, Mississippi State University, Mississippi State, Mississippi 39762, denver@cavs.msstate.edu

Andrew L. Bowman, Center for Advanced Vehicular Systems & Department of Mechanical Engineering, Mississippi State University, Mississippi 39762, alb494@msstate.edu

Noah Cho, Center for Advanced Vehicular Systems & Department of Computational Engineering, Mississippi State University, Mississippi State, Mississippi 39762, HeechenECho@gmail.com

Mark F. Horstemeyer, Center for Advanced Vehicular Systems & Department of Mechanical Engineering & Department of Computational Engineering, Mississippi State University, Mississippi 39762, mfhorst@me.msstate.edu

ABSTRACT

Finite element simulations of near impacts of terrestrial bodies are presented to investigate possible deformation behavior induced by a massive body during the creation week and/or Genesis Flood. Using the universal law of gravitation, a gravitationally loaded objected is subjected to the 'pull' of a near passing fly-by object, and the resulting surface deformations are studied. An Internal State Variable (ISV) pressure dependent plasticity model for silicate rocks (Cho *et al*., 2018) is used to model the deformation behavior and to capture the history effects involved during the complex surface loading/unloading found in a near impact event. The model is used to simulate the earth and a "fly-by" object interaction and is able to accurately reproduce the internal pressure profiles of the earth and fly-by object. In this context, the fly-by object can be the original Moon, a meteor, or another type of large object that has moved through space to interact with the Earth. Due to the wide range of features that can drive surface deformations during a near impact event, a Design Of Experiments (DOE) methodology was used to independently investigate the influences of five parameters (stationary body size, core material, core/mantle thickness ratio, passing object mass, and passing object distance) concerning surface deformation. The results indicate that the passing body distance, stationary body size, and core/mantle ratio are the most dominant influence parameters on surface deformation. Examination of the ISV parameters of the mantle during deformation shows a complex relationship between the hardening and recovery terms of the model and the resulting plastic strain and surface deformation induced from the near pass event. Surface rise from the near passage of a Moon sized object could be as high as 800 m, in turn causing large tsunamis and possibly causing the Earth's crust to crack. For this first of its kind study, the conclusions provide understanding of the possible ranges of deformations observed from a near pass event and provides insights into possible catastrophic deformation mechanisms relevant to the young Earth paradigm.

KEY WORDS

near impact, Finite Element Analysis, Internal State Variable Model, Genesis Flood

INTRODUCTION

With the recent exploration of the outer edge of our Solar System, a flurry of questions regarding planetary formation, heavy bombardment, Kuiper Belt objects, lunar formation and capture theories, and Solar System arrangement have been postulated within the secular research community. Thus, the proposed answers to these questions are entangled with Uniformitarian principles requiring millions or billions of years to explain the various phenomenon seen throughout the Solar System. From a Young Earth Creationist (YEC) standpoint, many of these phenomenon can only be explained from catastrophic processes occurring over relatively short time scales compared to those considered from the deep time uniformitarian perspective. The large evidences of Solar System wide cratering suggest that a Solar System wide catastrophe occurred, possibly related to the curse placed on the entirety of creation due to Adam's fall (Romans 8:20-22), extending to the Earth's catastrophic global flood, and extending further to future catastrophic events described during the final judgment (Revelation 8:8).

Models involving phenomenon on the planetary and solar system scales have traditionally fallen in two categories: impact event (Agnor et al. 1999; Quintana et al. 2016; Rickman et al. 2017) and rigid body dynamics (Nesvorný 2011; Pires et al. 2015). Impact studies assume all or most of the mass and energy are absorbed into the larger body. Studies on moving or orbiting bodies assume that all of the energy is conserved with the dynamics of motion and energy dissipation occurs through body deformation while plastic heating is not considered. Hence, there exists an intermediary between the two categories that has been explored very little; the near passage of n-bodies and the dissipative forces resulting from body deformation, body separation, or gravitational capture. The deformations potentially caused by near pass events has the potential to account for numerous phenomenon found throughout

the Solar System.

Very few studies have been performed on near passage interactions of bodies within the Solar System. In fact, of the studies that exist, none look at the body deformation induced by such a fly-by object event. Bate and Burkette (1997) used Smooth Particle Hydrodynamics (SPH) to investigate the self-gravity effects of a molecular cloud approaching a black-hole and showed the importance of considering self-gravity in close passage simulations. Hyodo et al. (2017) used SPH to investigate ring formation around giant planets from the near passing of a Kuiper Belt object. They showed that a majority of the mass of the Kuiper Belt object was captured by the planet but remained as large chunks in orbit around the planet. To the authors' knowledge, finite element simulations on fly-by near pass events has not been studied to date.

The largest body of work (model) making use of the modern tools and measurements has yielded to constraints aligned with the materialist paradigm of the current "Big Bang" cosmology and neo-Darwinian terrestrial biological evolution. These constraints demand that deep time be required on a cosmic time scale to allow for a random organization of structures on cosmic, galactic, and interstellar scales subject to the known laws of physics.

Models developed in recent years to address development of observed structures on the solar system scale (Pires et al. 2015) have introduced physically admissible limitations to the production of the observed configuration of our solar system structure. Models of uniformitarian planetary orbital evolution result in disruption and elimination of rocky planets in the inner Solar System by a process called resonance sweep. Attempts to bypass this stage of planetary orbital evolution, for example within the Nice model (Gomes et al. 2005; Tsiganis et al. 2005; Pires et al., 2015), have introduced catastrophic interactions to avoid the resonance sweep and preserve the derived structures of the inner Solar System. Notably, while the catastrophic interaction model (Nice) results from the cumulative disturbance of interactions with Jupiter, the catastrophic event occurs in a single orbit on the order of 50 years. The solution of a catastrophic interaction model addresses the question raised by observed cratering patterns on current solar system bodies attributed to and divided between the Early Heavy Bombardment (EHB) and the Late Heavy Bombardment (LHB).

The impasse of the orbital evolution question in the uniformitarian community touches on the question of the YEC community related to the natural order process time scale at work in the rest of the created order outside of our Solar System. It also raises the question of what physical events are admissible and consistent with the Biblical record of creation events and historical events recorded in the book of Genesis and referenced in other scriptures. For example, catastrophic processes have been proposed as a possible initiator to the Genesis Flood (Spencer 1998; Oard 2012) in the form of meteoric impacts providing the necessary energy to initiate plate subduction or by cracking the Earth's crust. Deformation from a near pass event could also create significant surface deformation and even unload portions of the Earth's crust allowing for rapid subduction to occur acting as a possible initiator to John Baumgardner's catastrophic plate tectonics model (Wise et al. 1994). However, evidence also shows that the Earth's mantle could have been created in such a way to trigger catastrophic plate subduction without the requirement of a triggering event (Horstemeyer and Baumgardner 2003). The near pass deformation alone could create large tsunamis carrying enough energy to transport large sediment deposits during the Genesis flood. Such a mechanism was hypothesized in a global sedimentation model proposed by Baumgardner (2013 and 2016).

Another problem confronting the planetary physics community is the history of formation of planets and satellites. The most glaring is the formation and history of the Earth and our Moon. There was a recent crisis from observations (Zhang, et al. 2012) that challenged the currently held view of lunar formation. Improved accuracy in isotope measurements allowed for separating meteoroids into distinct classes by isotopic composition, suggesting a signature of spatially distinct origin within the Solar System (according to the nebular hypothesis, which is based in the evolutionary paradigm). However, the new and more accurate measurements (Wiechert, et al. 2001; Zhang, et al. 2012) were retrieved from lunar samples, and the measurements indicated a statistically identical origin. This finding contradicted the long held lunar formation model (offset Thea impact model) caused by an impactor planet (Thea) fragmenting the Earth (Canup and Asphaug 2001).

The impact model of Canup and Asphaug preceded the development of the Nice model of Solar System evolution. The Canup and Asphau g model for lunar formation had the advantage of accounting for the current angular momentum of the Earth/Moon system and assumed a collision with a body that formed in the neighborhood of Earth, which later migrated into a relatively low velocity collision (escape velocity of earth ~5 km/s) with the Earth where the debris collected to form the Earth and our Moon. Current Solar System isotope composition models suggest that these bodies would have a small difference in their isotope signatures and old isotope measurements of lunar samples allowed for differences to fall within the measurement error bounds. However, the finding (Zhang et al. 2012) with improved precision indicates that the current Earth/Moon system formed from the same isotopic reservoir. Consequently, any impact theory of formation would need to fully vaporize and mix the isotopic reservoir that formed the Earth's mantle and moon.

Deformation occurring from near pass events could in theory, under certain fly-by scenarios, provide enough energy to unload a large enough portion of the body and cause separation to occur. This type of moon formation theory is much more difficult to model due to the requirement for momentum and energy to be conserved throughout the process for both the Earth and the close fly-by passing object. Such an event would likely have a large influence on the Earth's orbit, but the true effects are not known.

The impact models have an appeal as a mechanism on the uniformitarian timescale, because any impact will heat up the Earth and require a long time for the Earth's crust to cool. Elevating such formation scenarios necessarily contrast with current observations of cool solid bodies, logically demanding that formation must have occurred long, long ago. The wide spread cratering patterns observed among the solid bodies of the Solar System logically must follow the solidification period. Accumulating the time required to

solidify planetary bodies and subsequently absorb high numbers of impacting bodies culminates in deep time required to produce the observed structure and impact crater record.

Our work signifies an initial attempt to address the questions presented above and provide insights into the creation of the Solar System and possible catastrophic interactions occurring from the near passage of celestial objects related to the Earth. This first inception of the model aims to capture the body deformation induced by a passing object (moon, small planet, etc.) on a stable, orbiting object (Earth-like planet), in order to investigate factors contributing to the surface rise and overall deformation of the stationary body (Earth). Finite Element Analysis (FEA) on a planetary scale is cast in a Design of Experiments (DOE) framework to investigate the influence parameters on the Earth's surface deformation during a near pass fly-by. In particular, we focus on the Earth's deformations during near pass events as the size and position of the bodies are garnered from the current size and position of the Earth-Moon system. A complex thermomechanical Internal State Variable (ISV) elastic-plastic model is applied to allow for temperature dependent dissipation in the form of plastic deformation. Examination of the ISV parameters provide insights into the hardening and recovery related to dislocation mechanics and highlight certain areas pertaining to the highest rate of plastic deformation. Future model iterations will attempt to describe dissipation mechanisms from tidal and resonance heating and the angular momentum transfer that would occur given favorable conditions of a near pass event.

METHODS

1. Design of Experiments (DOE) Methodology

To provide a generalized understanding of the boundary conditions of our model, a split-level factorial DOE study is conducted to elicit the most essential aspects pertaining to a near pass event. The DOE presented herein studies the influence of five parameters related to the boundary conditions of a stationary object (body size, core material, and core/mantle thickness ratio) that represents the Earth and a passing object (object mass and passing distance) and the resulting influence on the stationary object's surface elevation change during a near pass event. A full factorial investigation at two levels would consist of thirty-two (2^5) unique simulations. A DOE analysis using an L_8 array can obtain the desired first order influences while reducing the number of simulations to eight calculations. The relationship between a set of influences, {A}, and responses, {R}, can be described by a linear mapping through the parameter matrix, [P], which corresponds to the chosen orthogonal array (L_8), as the following:

$$\{R\} = [P]\{A\}, \tag{1}$$

where {R}, {A}, and [P] are given in matrix form as:

$$\{R\} = \begin{Bmatrix} R_0 \\ R_1 \\ R_2 \\ R_3 \\ R_4 \\ R_5 \\ R_6 \\ R_7 \end{Bmatrix}, \{A\} = \begin{Bmatrix} A_0 \\ A_1 \\ A_2 \\ A_3 \\ A_4 \\ A_5 \\ A_6 \\ A_7 \end{Bmatrix}, [P] = \begin{bmatrix} +1 & -1 & -1 & -1 & -1 & -1 & -1 & -1 \\ +1 & - & -1 & -1 & +1 & +1 & +1 & +1 \\ +1 & -1 & +1 & +1 & -1 & -1 & +1 & +1 \\ +1 & -1 & +1 & +1 & +1 & +1 & -1 & -1 \\ +1 & +1 & -1 & +1 & -1 & +1 & -1 & +1 \\ +1 & +1 & -1 & +1 & +1 & -1 & +1 & -1 \\ +1 & +1 & +1 & -1 & -1 & +1 & -1 & +1 \\ +1 & +1 & +1 & -1 & +1 & -1 & +1 & -1 \end{bmatrix}$$

The magnitude of the set of influences, {A}, can be found by inverting the parameter matrix, [P], and solving

$$\{A\} = [P]^{-1}\{R\}.$$

For this study, three sets of responses, each targeting the surface elevation change at a specific surface area of the stationary body (Earth) are investigated. Figure 1 shows the model parameters for the DOE setup along with targeted areas of interest. The targets of interest correspond to local elevation change occurring on the approach surface, the near-side surface, and the out-of-plane direction. Table 1 describes the simulation parameter values used for the DOE with five parameters and two levels for each parameter. The parameters were chosen to be of similar size and composition to the Earth/Moon system.

2. Internal State Variable Model for Mantle Material

Many rheological mechanisms simultaneously operate in the Earth's mantle during deformation events. While many conceptual theories exist for mantle materials, the exact mechanisms involved and their relationship to mantle strengthening and weakening are still relatively unknown, especially when considering high rate deformation events. Most commonly, power-law creep models have been used to describe the mechanical responses of rock material. Such models rely on uniformitarian assumptions of very slow rates and are limited to few deformation mechanisms. With this motivation, several authors (Baumgardner 2003; Sherburn et al. 2011) have developed mathematical models to accurately and realistically describe some of the rheological mechanisms and have applied them to global mantle simulations, specifically regarding the dynamics of the Earth's mantle during the Genesis Flood.

Most recently, Sherburn et al. (2013) implemented the Internal State Variable (ISV) constitutive model, a sophisticated constitutive model originally developed at Sandia National Laboratories (Bammann 1990; Bammann et al., 1993; Horstemeyer 2000). The authors show that the ISV model has a great capacity of capturing the material behavior of metals, polymers, and mantle rocks. Through the use of internal state variables, the ISV model can capture the mechanical history of a material and be used to predict mechanical properties such as strength and deformation. Furthermore, the ISV model has the capability to accurately capture the elasticity and plasticity of a material, including the hardening and the recovery mechanisms related to internal structure rearrangement. Sherburn et al. (2013) discovered that a crucial microstructural mechanism dominated the Genesis Flood event: dynamic recovery. When the dynamic recovery was turned on in the calibrated ISV model using lherzolite's stress-strain data, simulations showed a significant strength weakening in the mantle. Because the catastrophic mantle deformation process during a near pass event would be much more dynamic than mantle motion we see today, the dynamic recovery or dislocation creep could be highly activated and greatly influence the resulting kinetics of planetary deformation.

A pressure dependent ISV model was implemented by Cho *et al.* (2018) to capture the complex mechanical behavior of the Earth's mantle in static and dynamic conditions. The ISV model is a strain-rate, pressure, and temperature dependent plasticity model that utilizes isotropic hardening as an internal state variable to describe dislocation pile up (hardening) and dislocation slip and

Table 1. Parameter matrix demonstrating the split level design of experiments simulation conditions.

Simulation	Core/Mantle Ratio	Stationary Body Size (m)	Passing Distance (m)	Core Material	Passing Body Mass (kg)
1	0.5 (-)	1.75E6 (-)	2.0E8 (-)	Olivine (-)	7.35E22 (-)
2	0.5 (-)	1.75E6 (-)	2.0E8 (-)	Iron (+)	5.97E24 (+)
3	0.5 (-)	6.37E6 (+)	4.0E8 (+)	Olivine (-)	7.35E22 (-)
4	0.5 (-)	6.37E6 (+)	4.0E8 (+)	Iron (+)	5.97E24 (+)
5	0.2 (+)	1.75E6 (-)	4.0E8 (+)	Olivine (-)	5.97E24 (+)
6	0.2 (+)	1.75E6 (-)	4.0E8 (+)	Iron (+)	7.35E22 (-)
7	0.2 (+)	6.37E6 (+)	2.0E8 (-)	Olivine (-)	5.97E24 (+)
8	0.2 (+)	6.37E6 (+)	2.0E8 (-)	Iron (+)	7.35E22 (-)

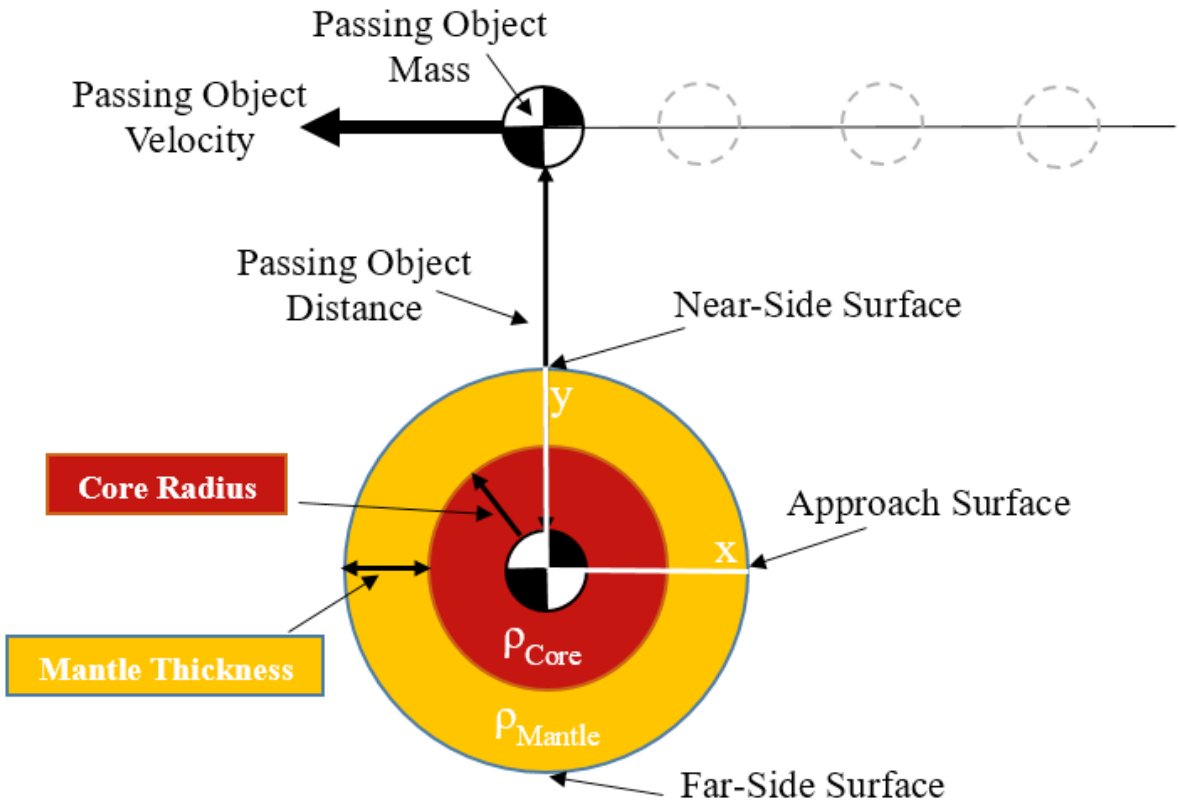

Figure 1. Model diagram illustrating the geometry, orientation, and motion of the deformable and passing bodies corresponding to adjustable parameters for the design of experiments analysis. Also illustrated are areas of interest pertaining to the approach surface (along x-axis), near and far side surfaces (along y-axis), and the out-of-plane surface deformation (along z-axis).

Table 2. Material constants for the mantle/core material used for the design of experiments simulation matrix. The ISV relates to the plasticity internal state variable constitutive model.

Layer	Material	Material Model	Temperature (K)	Density (kg/m^3)	Shear Modulus (GPa)	Bulk Modulus (GPa)
Mantle	Olivine	ISV	350	3345	80	130
Core	Olivine	Elastic	750	4500	80	130
Core	Iron	Elastic	2000	13000	176	1425

annihilation (recovery). The strain rate, pressure, and temperature dependence can be captured with sufficient experimental data for fitting. For this work, the ISV coefficients found in Cho et al. (2018) for polycrystalline olivine were used for the mantle material. The complete formulation for the ISV elastic-plastic model can be found in the same reference. The pressure dependent ISV model provides pressure sensitive descriptions of the yield surface and hardening equations, along with the bulk and shear modulus, to capture pressure effects on the dislocation mechanisms required for the extremely high pressures found in the Earth's mantle.

Regarding the yield surface in the present ISV constitutive model, Drucker-Prager shear failure yield surface and von Mises pressure insensitive yield surface were combined with Transitional yield surface to avoid numerical singularities (Hammi et al. 2016). This yield function describes that initially the elastic limit increases as pressure increases, but the elastic limit becomes insensitive to the pressure when the rock aggregate is fully compacted, as shown in several lab experiments (Kavner 2007).

Dislocation motion is also influenced by hydrostatic pressure. When the pressure increases, the activation barrier also increases; consequently, the dislocation mobility is somewhat suppressed. In the free energy concept, the pressure dependence of dislocation dynamics can be modeled via an activation volume (Karato 2012). Also, the current ISV formulism uses a pressure and temperature dependent shear modulus for the hardening moduli, and the shear modulus is estimated by 3rd-order Birch-Murnaghan equation of state. In this manner, the present ISV constitutive model captures the pressure dependent material's behavior, which counteracts against temperature effects.

3. Finite Element Analysis Setup

For this work, the finite element program ABAQUS/Standard v14.2 was used as the numerical code of choice. First, to validate the surface deformation predicted by the model, a simple Earth-Moon system was simulated to predict the surface deflection observed on the Moon by the Earth's gravitational pull. Both objects were stationary to simulate tidal locking between the Earth and Moon. The Moon sized object was first loaded under self-gravity then subjected to a gravitational body force according to Newton's law of gravitational acceleration and the resulting surface deformation was determined. The detailed procedures for the development and application of the self-gravity body force and the distributed gravitational body force are provided in the Appendix for reference. Figure 1 depicts the two-dimensional geometry, orientation, and trajectory of the stationary (Earth) and passing objects although the simulations were performed on a three-dimensional mesh. For the DOE simulations, the passing object travels within the x-y plane and begins at an x-distance of 1.4E10 m and travels at 7000 m/s in the negative x-direction. Table 2 lists material constants used for the olivine mantle/core and iron core. Due to the high pressure environment of the iron core, an elastic model was used to describe the core's material properties. The mantle material model was the ISV model for polycrystalline olivine described above.

For a detailed study of the near pass phenomena, the kinetics of a large object fly-by on a non-rotating two-layer model Earth were investigated for two cases. The first case is a Lunar scale mass (7.34 x 10^{22} kg) passing at a velocity of 5,000 m/s at a peri-apsis distance (point of nearest passage) of 45,000 km between mass centers. The second case is an Earth scale mass (5.97 x 10^{24} kg) passing at a velocity of 20,000 m/s and a peri-apsis distance of 45,000 km between mass centers. For both cases the passing body followed a simplified linear path with constant velocity in the equatorial plane of the model Earth.

The fly-by simulations occurred in two steps: first, a body force was applied to the stationary object to represent a self-gravitational load; second, a subsequent fly-by of a near pass object, modeled as a point mass, was passed by the stationary body at the prescribed velocity. The detailed procedures for the development and application of the self-gravity body force and the distributed body force due to the fly-by object are provided in the Appendix for reference. The following is a short description of the boundary conditions implemented for the simulation. To apply the self-gravity body force, an analytical expression based on the element radial distance was developed using Newton's law of gravitational acceleration. For the two-layer model, the self-gravity expression for the mantle became more complicated as it accounted for gravitational forces from the denser iron core and the olivine mantle. The distributed force expression for the gravitational force between the stationary and fly-by object used the ABAQUS user subroutine DLOAD. As shown in Figure 1, the passing fly-by object traveled at a constant velocity in a simplified linear path past the stationary object. Using the DLOAD routine, the position of the passing object was calculated at each time step and the distance was used in Newton's gravitational equations to calculate the resulting body forces on the stationary object. In order to remove the center of mass motion that was created from the pull of the passing object, the ABAQUS inertia relief command was used and only body deformation was allowed. All geometries resulting from the DOE setup are meshed with three-dimensional, twenty-noded, continuum, quadratic, brick elements with reduced integration (C3D20R). The global size of elements for each simulation was 250 km.

Post-processing of the simulation data was performed with ABAQUS/CAE v14.4. To study the effect of self-gravity, pressure

contours were generated and pressure versus surface depth graphs were constructed. During the fly-by event, von Mises stress contours were generated at equal intervals from 0 seconds to 20,000 seconds in order to show the stress state changes. The surface displacement history on the approach face, the near-side face, and the out-of-plane direction (Poisson's contraction) are plotted at several intervals throughout the fly-by. Contour plots of the plastic strain and isotropic hardening are also presented at equal intervals from 0 seconds to 20,000 seconds to provide insight into the hardening mechanisms involved during the near pass event.

RESULTS/DISCUSSION

1. Model Validation with Earth-Moon System

The model validation procedure for the near impact event includes comparing the pressure profiles and surface deformation of known quantities within the Earth-Moon system. Since the early solar system history is of interest, especially related to possible Earth-Moon interactions, careful attention is given to the pressure profile of the Earth due to self-gravity. The importance of capturing the self-gravity loading is expressed during the unloading of stress that occurs during a near pass event. If the stationary body is initially unloaded or loaded insufficiently, the magnitude of surface deformation will be difficult to determine. Figure 2 illustrates the simulated two-layer Earth pressure response due to self-gravity forces. The complete pressure profile is shown in Figure 2(b) and is compared to the Preliminary Earth Reference Model (PREM) pressure profile obtained from seismic data (Dziewonski and Anderson 1981). The PREM model is a popular one-dimensional model fit from seismic data of the Earth's layers and the first model to account for attenuation and anisotropy within the Earth. However, the PREM model is a zeroth order approximation due to the ellipticity and lateral variations within layers of the Earth, which poorly represents some areas of the uppermost and lower mantle. Thus, the model represents averages over the heterogeneous structure of the Earth.

The overall pressure profile of the Earth is well captured throughout the mantle and core. The transition from the rocky mantle to the iron core is captured in the model by the sudden increase in pressure at the core-mantle boundary. Figure 3 compares the pressure dependence of the density, bulk modulus, and shear modulus to the PREM model within the mantle. The density profile is well predicted through the mantle. The bulk modulus and shear modulus are observed to be pressure dependent and compare well to the PREM model up to a depth of 600 km. At around 600 km, the crystallographic structure of the mantle rock changes causing a rapid increase in bulk modulus and shear modulus, an effect not captured by our model and illustrates the complexity involved in capturing the compete mantle behavior. Although a precise fit of the moduli is not achieved, the pressure and density profiles are well predicted.

The next step in the simulation process is to compare the simulated lunar pressure and lunar tidal bulge to the experimentally determined values. Figure 4 illustrates the simulated lunar pressure profile due to self-gravity loading. While the complete pressure profile of the moon has not been experimentally determined, the maximum pressure of the moon is estimated to be five to six GPa through seismic experiments (de Vries et al. 2010). The estimated maximum lunar pressure compares closely to our simulated maximum pressure of 6.6 GPa. Additionally, the lunar tidal bulge created by the gravitational pull of the Earth was calculated. From the simulation, the bulge was calculated to be 87.5 cm and is within the experimental uncertainty bounds of 52 cm ± 126 cm determined recently by NASA measurements (Mazarico et al. 2014).

2. Design of Experiments Results

The results of the normalized influence of the parameters on the approaching face surface deformation are shown in Figure 5. Based on the results, the dominating influences are the passing object distance, stationary body size, and the core/material ratio. The greater influence of these three parameters indicates that the surface rise on the approaching face is greatly dependent on the increased self-gravity loading caused by a much denser iron core and a larger iron core radius. The presence of a large dense core produces large gravitational forces that must be overcome to unload the surface and cause deformation during a near pass event. The core materials, along with a passing body mass, moderately influence the surface rise as they are directly involved in Newton's equation in determining the force between the two bodies. Figure

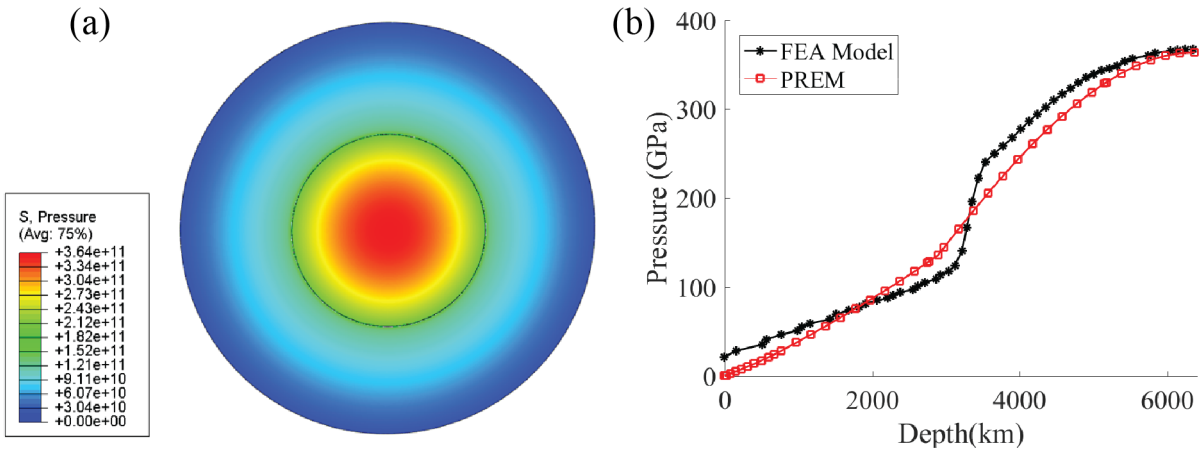

Figure 2. Internal pressure of a two-layer earth model (iron core, olivine mantle) due to self-gravity illustrating a) the finite element analysis pressure contour and b) the simulated internal pressure profile compared to the Preliminary Reference Earth Model (PREM) (Dziewonski and Anderson, 1981).

6 depicts the influence on the near-side surface rise during a near pass event. The surface rise on the near-side has similar influences as the surface rise on the approaching face. However, the surface rise on the far-side face, seen in Figure 7, received only a slight influence from the core material and passing body mass and is driven mainly by the passing object distance, stationary body size, and the core/material ratio. Additionally, the large deformation on the near-side causes a Poisson contraction on the other faces, which is largely dominated by the material properties of the stationary body.

To illustrate the effects of a Poisson's contraction on the stationary body rise, the influence of the out-of-plane deformation is shown in Figure 8. Similarly, the dominating influences are the passing object distance, stationary body size, and the core/material ratio. The core material and passing body mass have lower order influence on the deformation, the latter of which is related to the geometry and material properties of the stationary body, which would naturally have significant influence on the Poisson effect giving the out-of-plane deformation.

3. Detailed Examination of Near Pass Phenomenon

The two cases chosen for a detailed examination of near pass phenomena are inspired by the rocky inner planets of our Solar System. The primary body is two-layered with Earth sized dimensions and mass distribution. The near pass body masses reflect a large mass difference (case one with 100:1 mass ratio) and an equal mass interaction (case two). The near pass velocities represent a slow approach (case one at 5,000 m/s) consistent with an interaction between a rocky planet with similar orbits, and a fast approach (case two at 20,000 m/s) consistent with interactions of high eccentricity orbits crossing with inner Solar System bodies.

A. Case I: Near Pass of Lunar Mass Object

Figure 9 illustrates the surface elevation change during a near pass event of a moon sized object at several locations of interest (points A-E) along the stationary body (earth). Figure 9a shows the surface elevation change for a simulation where the mantle layer is modeled as a linear elastic material with a constant, pressure independent elastic modulus and no permanent plastic deformation. This simulation allows us to see the surface rise from the elastic unloading effect as the gravitational field from the passing mass modifies the self-gravity field for every element in the model Earth. Initially, at the early stages of the fly-by approach, the surfaces at points A, B, C, and D began to expand, while the out-of-plane surface at E began to contract. As the passing object approaches the point of nearest passage, the maximum surface elevation changes occur at the near and far-side (points C and D), while the surfaces at A and B and the out-of-plane surface at E, contracted to form the egg-like mode shape due to a Poisson's effect. Due to this contraction, there exists a drastic elevation change from point A to point C and would cause significant tidal disturbances worldwide during such an event. The wall of water generated by the near pass would be close to the same magnitude required (2500 m) from John Baumgardner's large-scale sedimentation model (Baumgardner 2013) and could provide a mechanism for understanding the sediment sequences covering the surface of the Earth. It is important to note that the movement of water in this scenario would not be due primarily to a change in tidal acceleration experienced by water molecules within the oceans, but rather from the shape change of ocean basins containing the water due to elastic unloading of the entire mantle of the model Earth.

Figure 9b shows the surface elevation change for a simulation where the mantle layer is modeled as an elastic/plastic material with temperature and pressure dependent elastic modulus and yield surface. In contrast with the elastic simulation, where surface points returned to their original elevations after the near pass event, the elastic + plastic simulation retains permanent body deformation from flow within the mantle that combines to retain a surface elevation change after the near pass event. Figure 10 shows the total displacements at five time steps during the near passage for an equatorial cross section of the model Earth. These displacements include the elastic distortion and the plastic flow. The final frame of Figure 10 labeled 20,000 seconds (5.5 hours) after time of

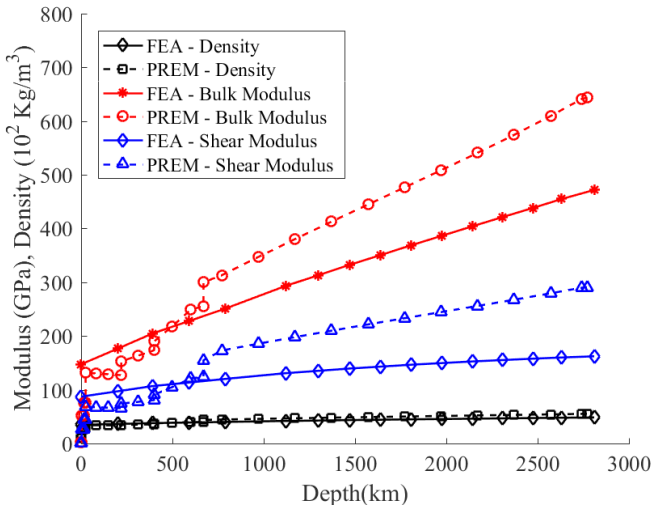

Figure 3. Comparison of the simulated pressure dependent density, bulk modulus, and shear modulus profiles to the Preliminary Reference Earth Model (PREM) (Dziewonski and Anderson, 1981) through the mantle depth.

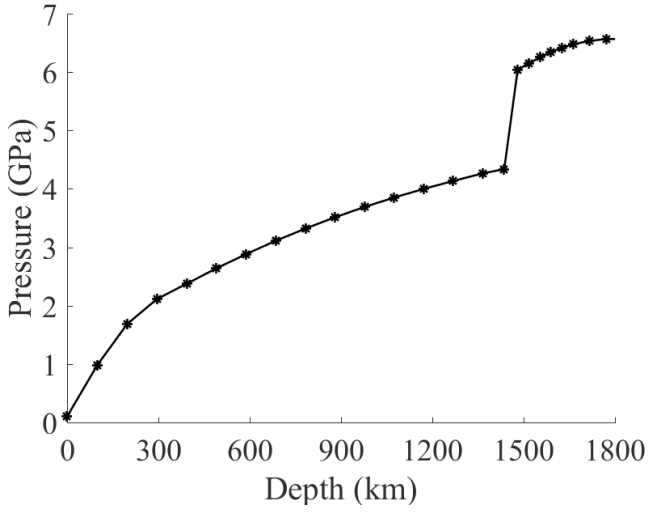

Figure 4. Simulated internal pressure profile of the two-layer moon sized object model (iron core, olivine mantle) due to self-gravity.

nearest passage shows the distribution of permanent displacement due to plastic flow. Figure 11 shows the effective plastic strain for the same section but restricted to the mantle layer for five time steps during the fly-by. The early plastic strains are distributed through the full mantle beneath the approach-side face, A, with the largest plastic strains near the core/mantle interface. The plastic strain spreads around the mantle toward the near-side face, C, but to a lesser degree. This difference in plastic strain at later intervals could be due to the hardening induced in the mantle region on the approach-side face inhibiting the later flow into the near-side region. The difference could also be due to the higher strain rate during the near passage phase, although the closer distance at time of nearest passage produces a larger driving force. Figure 12 shows the isotropic hardening (κ) distribution for an equatorial section of the mantle layer for five time steps during the fly-by. The region of highest hardening is adjacent to the core/mantle interface near the approach side and adds 10 MPa to the initial yield surface. The use of a complex ISV elastic-plastic model for the mantle allows for a more detailed understanding of the mantle's response to deformation. With the current model, isotropic hardening (κ) is the critical ISV for influencing the resulting deformation through dislocation build up and recovery. Kinematic hardening values are approximately 20% of isotropic hardening. The evolution of the isotropic hardening variable is depicted in Figure 12.

Modern tsunamis are generated during an earthquake when the elastic strain energy stored in the oceanic crust is relieved by a rupture causing a net change in ocean basin volume or morphology. Figure 9a and b shows the relative displacement of the model Earth surface points at 90 degrees of longitudinal separation. If a pre-flood ocean basin were to span these regions during a lunar mass fly-by, the effect would be analogous to lifting one edge of the ocean floor basin by as much as 400 meters at the peak of the transient and as much as 200 meters in permanent relative offset. While the primary question for this first case related to the possible role in flood initiation or providing a driving force for ocean water inundation, the most remarkable observation is the global pattern of elevation change. Figure 13 shows a spherical map of permanent radial displacement ranging from 120m below to 120m above the initial body surface. Even though the largest local plastic deformation was 360 μm/m (0.036% strain), the cumulative effect

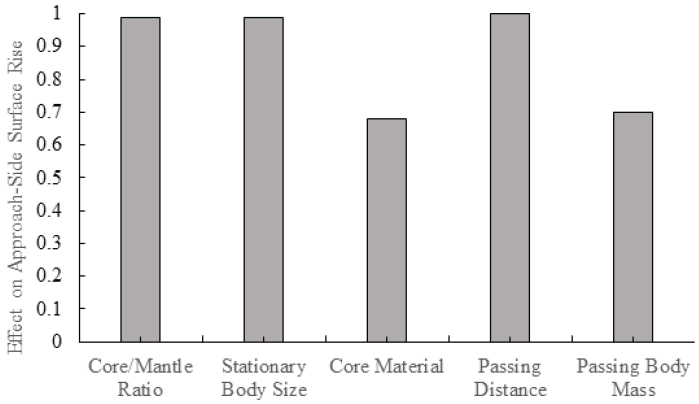

Figure 5. Normalized influence of each design of experiment parameter related to the surface deformation of the approach face of the stationary body (earth). The results show that the passing object distance, stationary body size, and the core/material ratio have a first order parametric influence on the surface deformation.

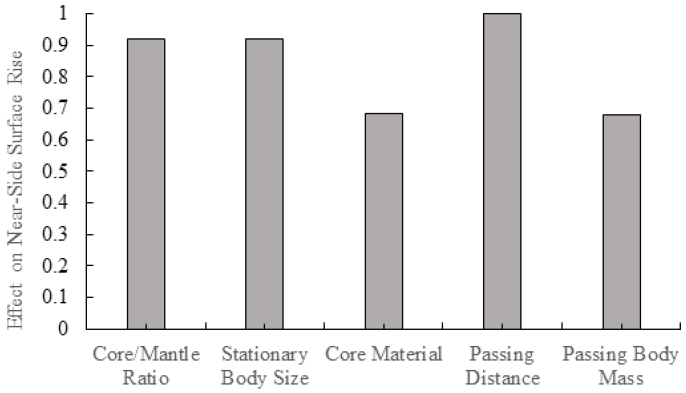

Figure 6. Normalized influence of each design of experiment parameter on the surface rise of the near-side face of the stationary body (earth). Note that the passing object distance, stationary body size, and the core/material ratio all were first order influence parameters.

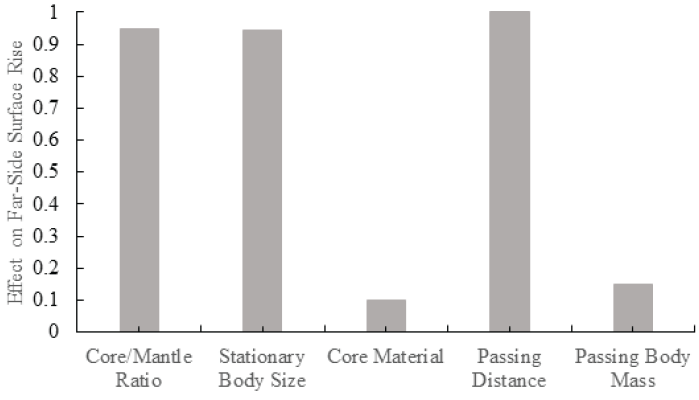

Figure 7. Normalized influence of each design of experiment parameter on the surface rise of the far-side of the stationary body (earth). Note that the passing object distance, stationary body size, and the core/material ratio all were first order influence parameters.

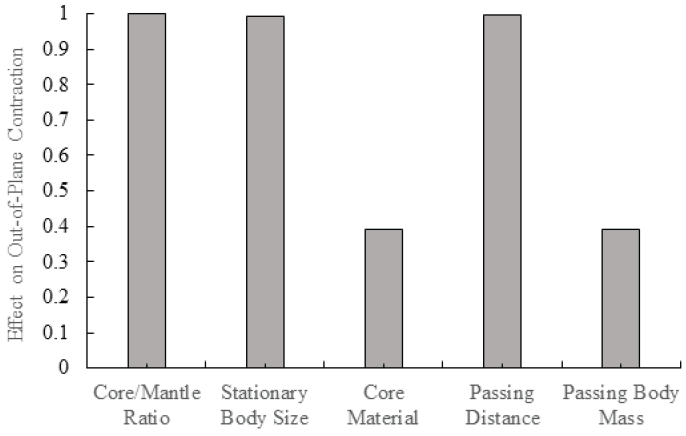

Figure 8. Normalized influence of each design of experiment parameter on the out-of-plane contraction of the stationary body (earth). Note that the passing object distance, stationary body size, and the core/material ratio all were first order influence parameters.

through the mantle results in a global highland region with two peaks each spanning 30 steradians and a band of lowland stretching along the far-side between the passage axis poles.

B. Case II: Near Pass of Earth Mass Object

The second case considers the passage of an Earth mass object passing at a distance of approximately 3 diameters which is outside the roach limit for rocky planets. During the course of fly-by, the model Earth began to elongate in an egg-like shape and followed the passing object's trajectory. As the passing object begins to retreat from the stationary body, large amounts of hardening and plastic deformation accumulate on the approach and near-side face, suggesting that the majority of the plasticity response occurs within the approach side of the fly-by object. The distinction of case II is immediately apparent in the total displacements shown in Figure 14 compared to Figure 10 for case I. The largest residual displacements vectors after passage occur between the near-side and retreat-side and follow nearly parallel to the surface resulting in approximately 60 km of lateral displacement.

Figure 15 shows the Von Mises stress for an equatorial section of the mantle layer for 5 time steps during the Earth mass passage. The initial frame, labeled -10,000 seconds before nearest passage, is shown retaining the Mises stress from the initial gravitational loading step unlike Figure 16 where the plastic strains from the initial gravitational loading step have been removed. Comparing the second frame from Figure 14, Figure 15 and Figure 16, labeled -2,500 and -5,000 seconds, as mantle material flows away from the far-side and retreat-side face, the Mises stress decreases while no plastic strain occurs. At the same time, mantle material flows toward the approach-side face where Mises stress rises above yield and plastic strain begins. Figure 16 demonstrates the evolution of the plastic strain accumulated from the hardening response during the near pass event. Figure 17 shows the progression of isotropic

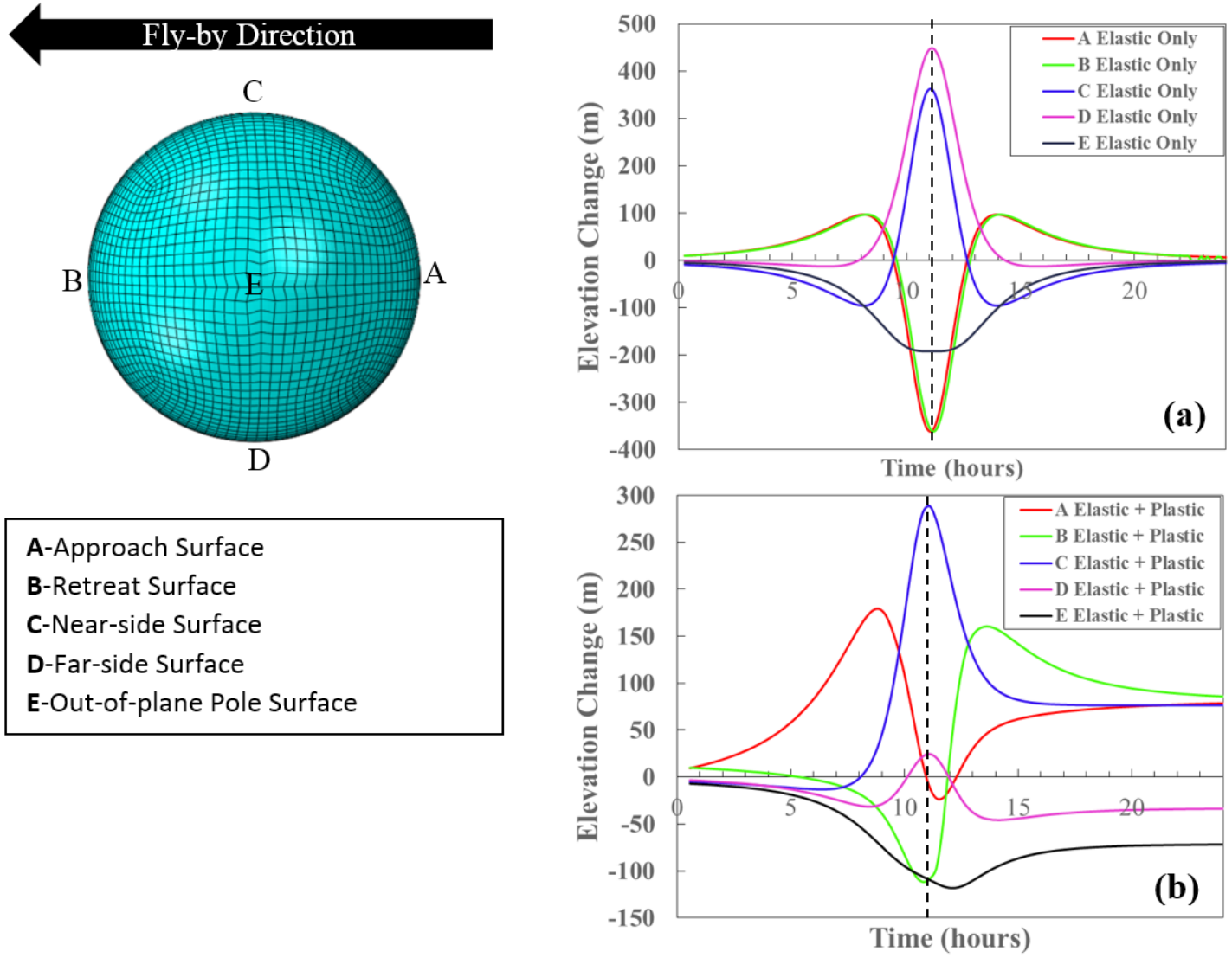

Figure 9. The stationary body (model Earth) surface elevation change of reference points during the near pass of a lunar mass object over a 24 hour timespan for (a) linear elastic mantle material and (b) elastic/plastic ISV mantle material with pressure/temperature dependent elastic moduli. The magnitudes of elevation change are reduced using the pressure dependent ISV model and show permanent deformation. The dashed line indicates time of nearest passage point (peri-apsis distance of 45,000m) for both simulations. Surface reference points A and B are the approach and retreat faces, C and D are the near and far side faces, and E is the out-of-plane polar contraction face.

hardening as the Earth mass object passes nearest approach. In contrast to case I, where the maximum isotropic hardening is 10 MPa, for case II the maximum is 1.9 GPa occurring at just above the core/mantle boundary between the near-side and retreat-side. The maximum strain rate ($3.5x\ 10^{-6}\ s^{-1}$) also occurred in the same region. The distribution of kinematic hardening for case II follows the pattern of case I, initiating on the approach side near the core/mantle interface. Ratio of the passing masses for case II to case I is approximately 100 as is the ratio of isotropic hardening and plastic strain. However, the case II to case I ratio of radial surface displacement is 200.

The most striking feature of the case II simulation is the stark global relief pattern remaining when the transient elastic loading from the fly-by has dissipated. Figure 18 shows the permanent radial displacement after passage of the fly-by Earth mass. The color map on projected hemispheres shows elevations ranging from 21,500 meters above to 9,000 meters below the original surface of the model Earth. Like case I, in Figure 18 a global pattern of highlands and lowlands is visible.

The planet Mars is a Solar System body that exhibits a global trend of highlands and lowlands. Figure 19 shows the topography map of Mars collected by the Mars Global Surveyor experiment (NASA/JPL) projected onto a sphere. The Sphere was oriented to best match the patterns from the case II simulation. The near passage pole is oriented approximately 50 degrees from the rotation axis of Mars. The case II simulation applied a passing velocity of 20,000 m/s where most of the plastic deformation took place within 2 hours surrounding the time of nearest passage. The case I simulation was slower at 5,000 m/s allowing an 8 hour window to induce the global deformation pattern. Both case I and II were applied to non-rotating models. The current rotation of Mars is 24.4 ±0.05 hours. If the analog from case II holds for the near passage of a Martian

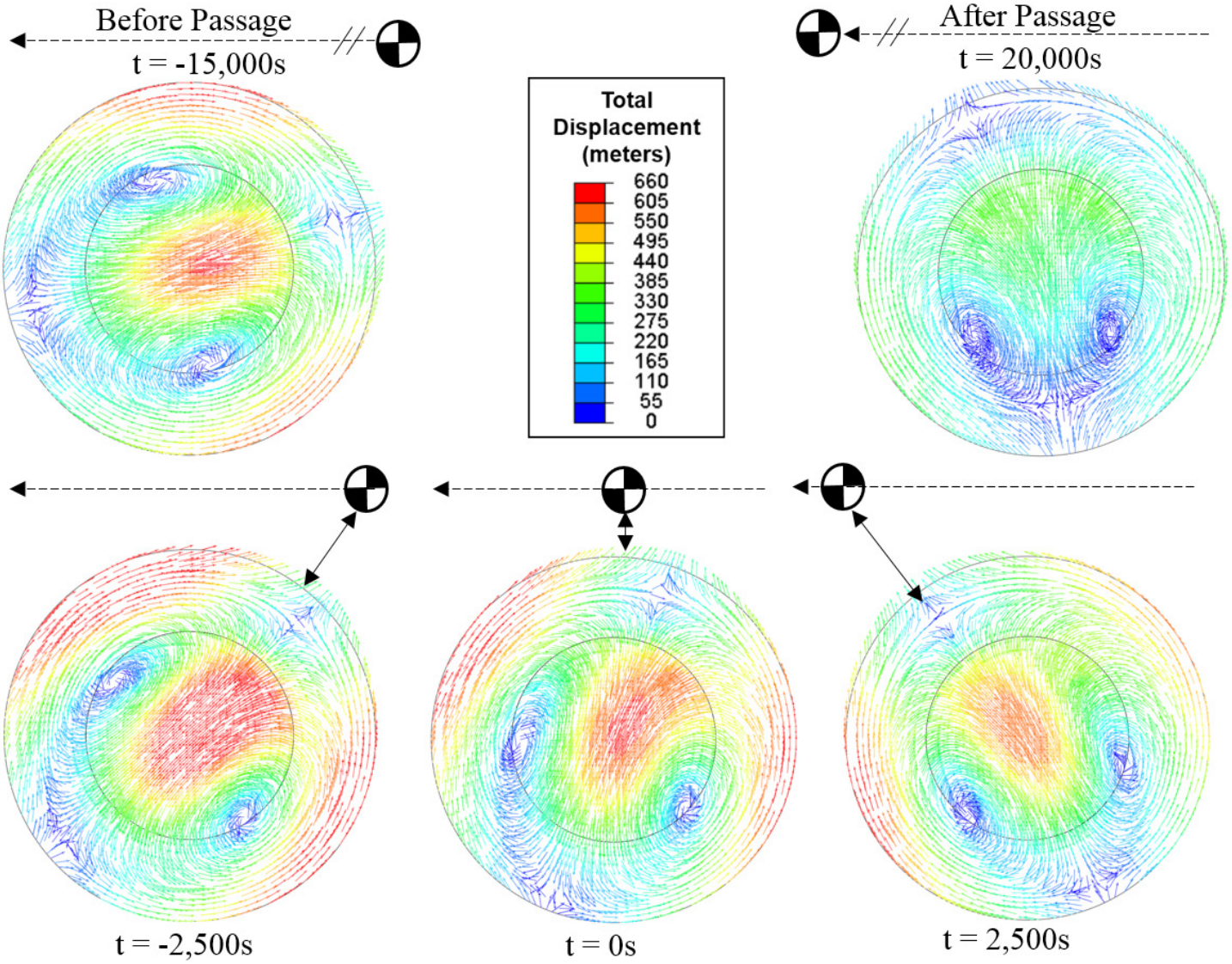

Figure 10. Cross sectional view of the stationary body (model Earth) along the equatorial x-y plane showing the total displacement occurring during fly-by for both mantle and core material. Counter clockwise from the upper left are shown displacements at time steps referenced to time of nearest passage. The position of the fly-by mass is shown as it passes above the stationary object from right to left (indicated by arrows). Note the presence of residual displacements after passage.

model, a Mars size mass passing at a velocity of 10,000 ±5,000 m/s at a peri-apsis of 3 diameters (20,000 ±5,000 km) could induce the global pattern of highlands and lowlands observed today. It is possible that heat generated from the plastic deformation of a near passage was sufficient to generate large partial melt reservoirs from which the widespread volcanism observed on Mars may have been derived.

C. Biblical Significance of a Near Pass Event

The biblical significance of the near pass events studied in this work present themselves in four main ways: continental deformation and movement during the creation week, as a precursor or initiator to the global flood, and as a possible mechanism to the large continental sedimentation and erosion in the period after the flood, and possible Solar System events occurring during the creation week or during the global flood. The creation of celestial objects on Day Four have unknown consequences but it is conceivable that a large amounts of Solar System activity occurred and could cause some sort of geological effect during this phase. Activity realized in this time frame could also be a precursor to future cataclysmic events.

The possibility of a near pass event being involved with the initiation or post-initiation events during the global Genesis flood has been theorized in many forms (Baumgardner 2013). Not considering the problems that must be overcome with such a model, the tidal disturbances created from a near pass event would cause massive tsunamis that would sweep over the continental surfaces, and could be responsible for inundating the continents causing erosion and sedimentation. Additionally, areas of unloading and residual displacement, as shown in Figures 10 and 15, could act as initiators to plate subduction in the Catastrophic Plate Tectonics model (Baumgardner 2003). Hence, an unknown interaction with the Moon or some fast moving celestial object could in fact set in motion the great Flood events.

CONCLUSIONS

The deformation induced from a near pass between two celestial objects was simulated using finite element analysis coupled with

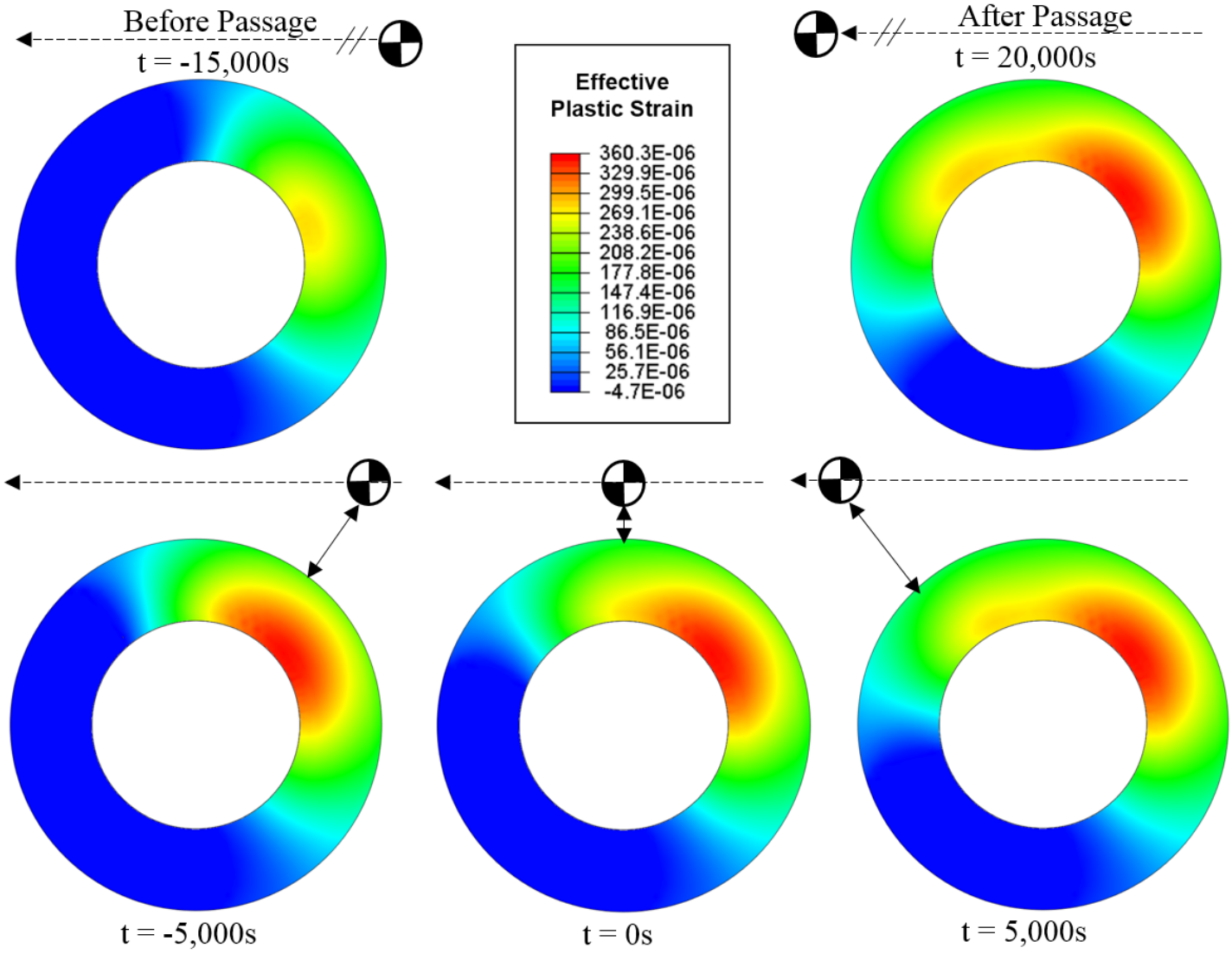

Figure 11. Equivalent plastic strain for cross sections of the stationary body (model Earth) along the equatorial x-y plane calculated from the internal state variable elastic-plastic model used for the mantle material. Counter clockwise from the upper left are shown total plastic strain at time steps referenced to time of nearest passage. All plastic strains were reset to zero at beginning of the simulation step (-20,000 seconds).

a strain-rate and temperature dependent plasticity ISV model with temperature and pressure dependent moduli and yield surfaces. A DOE study was conducted to study the critical parameters influencing the surface rise and fall during a near pass event. The study revealed that the core material and core/mantle ratio are critical parameters for surface deformations occurring on all faces of the body and along with body size are the driving factors behind the Poisson's contraction observed in the out-of-plane direction. The surface elevation change during the near pass of a moon sized object would cause a large surface rise (400 m) inevitably creating large tsunamis and causing large sedimentation on the continent surfaces. Detailed insights into the plastic response of the mantle are investigated through the evolution of ISV parameters and show that isotropic hardening and recovery lead to the permanent plastic deformation observed on the leading surface of the body potentially nucleating cracks in the Earth's crust.

This work introduces a framework for the investigation of dissipation mechanisms associated with near pass events within the Solar System. The incorporation of an ISV model allows for the plastic behavior to be determined, subsequently allowing for the heat generation due to plastic deformation to be accounted for during near pass, tidal, and/or resonance disturbances and a host of other boundary value problems involving gravitational disturbances and their resulting deformations.

REFERENCES

Agnor, C. B., R.M. Canup, and H.F. Levison. 1999. On the character and consequences of large impacts in the late stage of terrestrial planet formation. *Icarus* 142, no. 1: 219-237.

Bammann, D.J. 1990. Modeling temperature and strain rate dependent large of metals. *Applied Mechanics Reviews* 43, no. 5: 312-319.

Bammann, D.J., M.L. Chiesa, M.F. Horstemeyer, and L.I. Weingarten. 1993. Failure in ductile materials using finite element methods. *Structural Crashworthiness and Failure*, eds. T. Wierzbicki, and N. Jones, Elsevier Applied Science, The Universities Press (Belfast) Ltd.

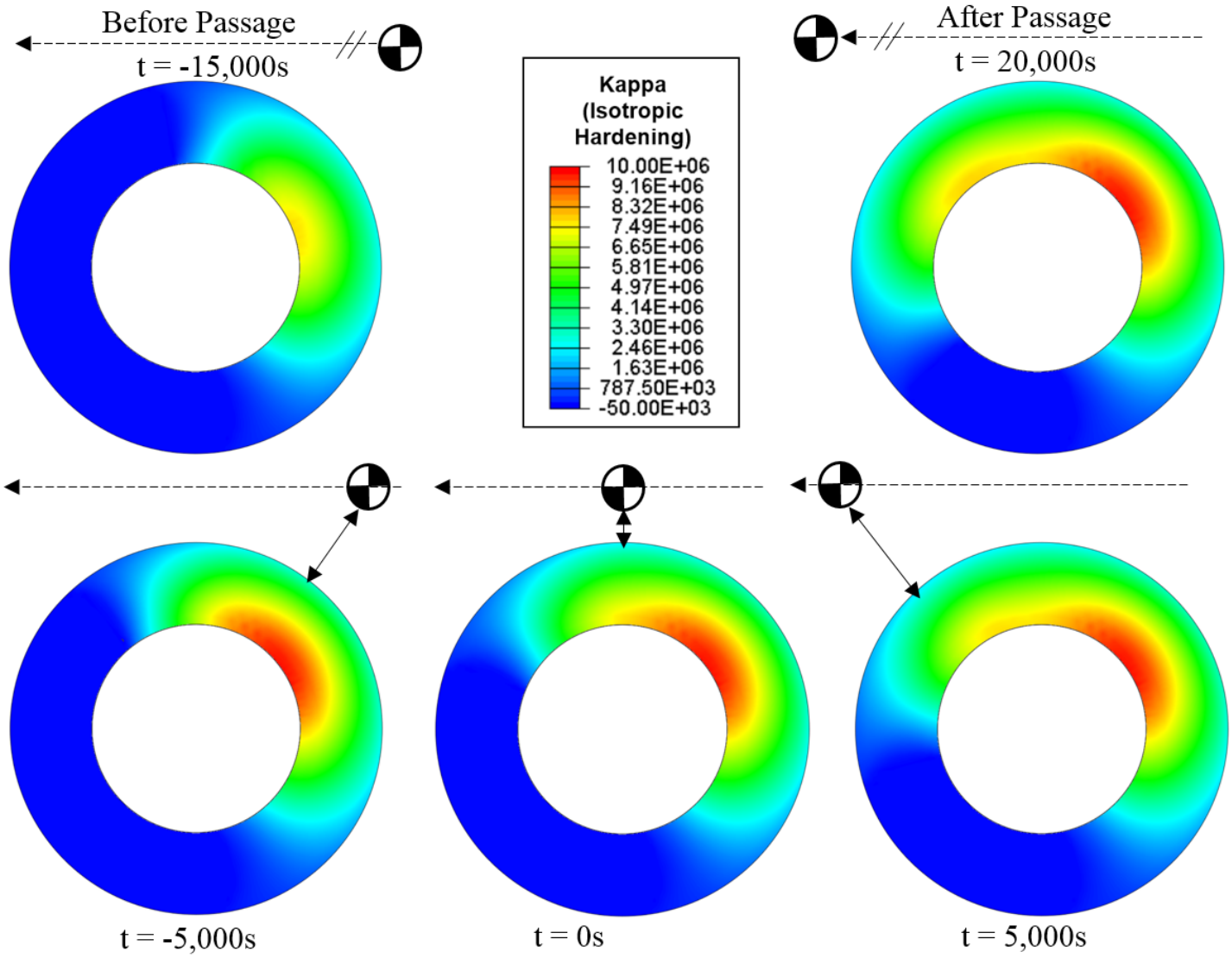

Figure 12. Isotropic hardening (kappa or SDV7) for cross sections of the stationary body (model Earth) along the equatorial x-y plane calculated from the internal state variable elastic-plastic model used for the mantle material. Counter clockwise from the upper left are shown isotropic hardening at time steps referenced to time of nearest passage. The pattern is not symmetric about the plane of nearest passage, but matches closely with the equivalent plastic strain.

Bate, R.M., and A. Burkert. 1997. Resolution requirements for smoothed particle hydrodynamics calculations with self-gravity. *Monthly Notices of the Royal Astronomical Society* 288, no 4: 1060-1072.

Baumgardner, J.R. 2003. Catastrophic plate tectonics: the physics behind the Genesis Flood. In *Proceedings of the Fifth International Conference on Creationism*, ed. R.L. Ivey, Jr., pp. 113–126. Pittsburgh, Pennsylvania: Creation Science Fellowship.

Baumgardner, J.R. 2013. Explaining the continental fossil-bearing sediment record in terms of the Genesis Flood: insights from numerical modeling of erosion, sediment transport and deposition processes on a global scale. In *Proceedings of the Seventh International Conference on Creationism*, ed. M.F. Horstemeyer. Pittsburgh, Pennsylvania: Creation Science Fellowship.

Baumgardner, J.R. 2016. Numerical modeling of the large-scale erosion, sediment transport, and deposition processes of the Genesis Flood. *Answers Research Journal* 9: 1-24.

Canup, R., and E. Asphaug. 2001. Origin of the Moon in a giant impact near the end of the Earth's formation. *Nature* 412: 708-712.

Cho, H., M. Horstemeyer, J. Baumgardner, and J. Sherburn. 2018. Strength-reducing mechanisms in mantle rock during the Genesis Flood. In *Proceedings of the Eighth International Conference on Creationism*, ed. J.H. Whitmore, pp. 707-730. Pittsburgh, Pennsylvania: Creation Science Fellowship.

Cuk, M. and, S.T. Stewart. 2012. Making the moon from a fast-spinning earth: a giant impact followed by resonant despinning. *Science* 338, no. 6110: 1047-1052.

de Vries, J., A. van den Berg, and W. van Westrenen. 2010. Formation and evolution of a lunar core from ilmenite-rich magma ocean cumulates. *Earth and Planetary Science Letters* 292, no. 1: 139-147.

Dziewonski, A.M., and D.L. Anderson. 1981. Preliminary reference Earth model. *Physics of the Earth and Planetary Interiors* 25: 297-356

Gomes, R., H.F. Levison, K. Tsiganis, and A. Morbidelli. 2005. Origin of the cataclysmic Late Heavy Bombardment period of the terrestrial planets. *Nature* 435: 466–469.

Hammi, Y., T.W. Stone, B. Paliwal, M.F. Horstemeyer, and P.G. Allison. 2016. Smooth yield surface constitutive modeling for granular

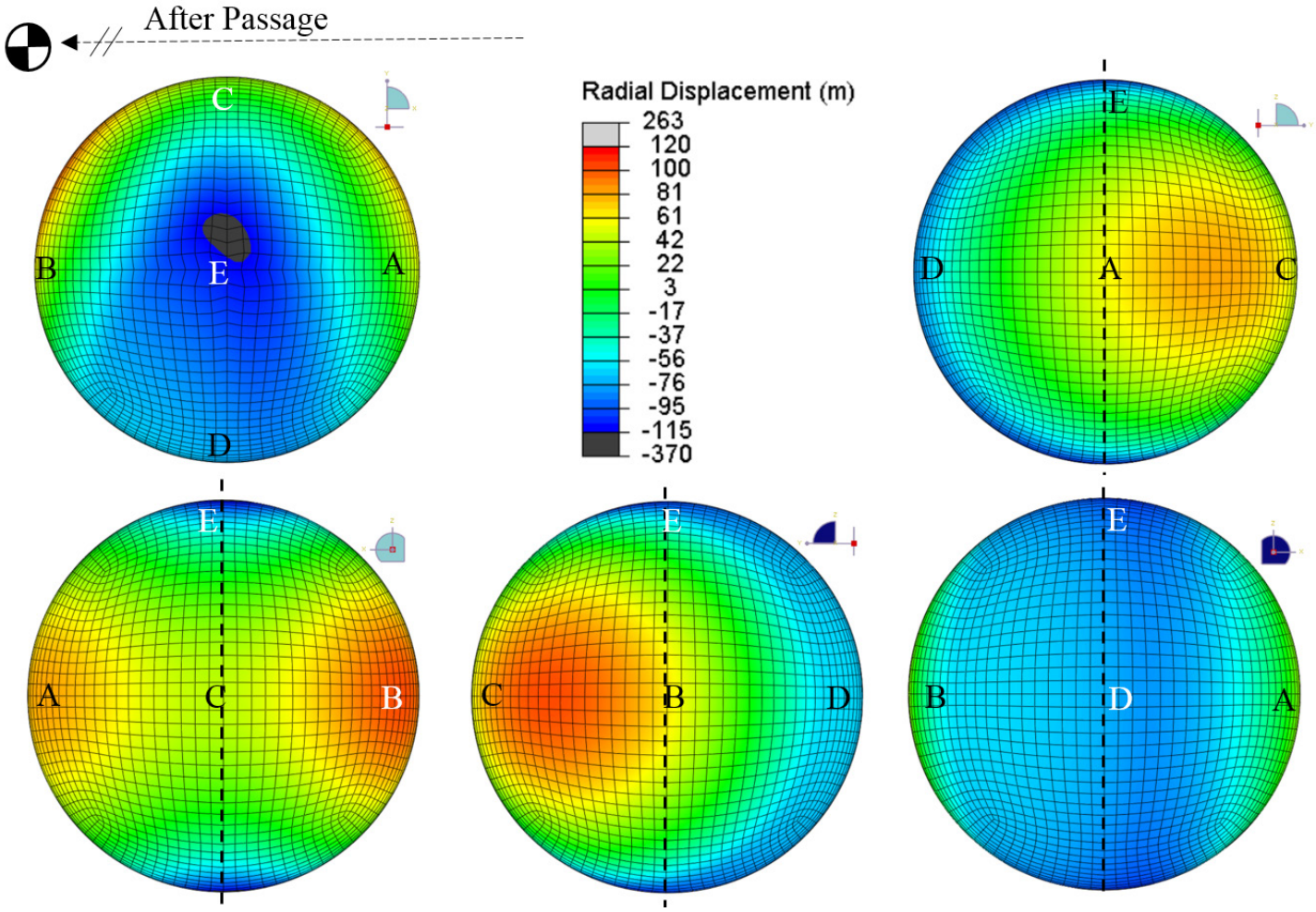

Figure 13. Global map of permanent radial displacements for a two-layer Earth size model after near passage of a lunar mass object. The color coding indicates permanent topographical change after subsidence of the transient elastic displacements. Counter clockwise from the upper left are shown: (E) polar view, equatorial views of (C) near-side surface, (B) retreat-side surface, (D) far-side surface, and (B) approach-side surface. The value of the displacement is relative to the original surface as measured from the geometric center of the body. Note the global pattern of highlands (greens through red) and lowlands (blues), there are two elevated peaks and a band of lowlands stretching from pole to pole around the far-side.

materials. *Journal of Engineering Materials and Technology* 139, 011010-011010–10.

Horstemeyer, M.F., J. Lathrop, A.M. Gokhale, and M. Dighe. 2000. Modeling stress state dependent damage evolution in a cast Al–Si–Mg aluminum alloy. *Theoretical and Applied Fracture Mechanics* 33:31–47.

Horstemeyer, M.F., and J.R. Baumgardner. 2003. What initiated the Flood cataclysm? In *Proceedings of the Fifth International Conference on Creationism*, ed. R.E. Walsh., pp. 155-163. Pittsburgh, Pennsylvania: Creation Science Fellowship

Hyodo, R., S. Charnoz, K. Ohtsuki, and H. Genda. 2017. Ring formation around giant planets by tidal disruption of a single passing large Kuiper belt object. *Icarus* 282: 195-213.

Karato, S. 2012. *Deformation of Earth materials.* Cambridge University Press.

Kavner, A. 2007. Garnet yield strength at high pressures and implications for upper mantle and transition zone rheology. *Journal of Geophysical Research: Solid Earth* 112, B12207.

Mazarico, E., M.K. Barker, G.A. Neumann, M.T. Zuber, and D.E. Smith. 2014. Detection of the lunar body tide by the Lunar Orbiter Laser Altimeter. *Geophysical Research Letters* 41, no. 7: 2282–2288.

NASA/JPL. Mars topographic map. Mars Global Surveyor. Mars Orbital Laser Altimeter.

Nesvorný, D. 2011. Young solar system's fifth giant planet? *The Astrophysical Journal Letters* 742: L22.

Oard, M.J. 2012. An impact Flood submodel—dealing with issues. *Journal of Creation* 26, no 2: 73-81.

Pires, P., S.M. Giuliatti Winter, and R.S. Gomes. 2015. The evolution of a Pluto-like system during the migration of the ice giants. *Icarus* 246: 330-338.

Quintana, E.V., T. Barclay, W.J. Borucki, J.F. Rowe, and J.E. Chambers. 2016. The frequency of giant impacts on Earth-like worlds. *The Astrophysical Journal* 821, no. 2: 126-139.

Rickman, H., T. Wisniowski, R. Gabryszewski, P. Wajer, K. Wojcikowski, S. Szutowicz, G.B. Valsecchi, and A. Morbidelli. 2017. Cometary impact

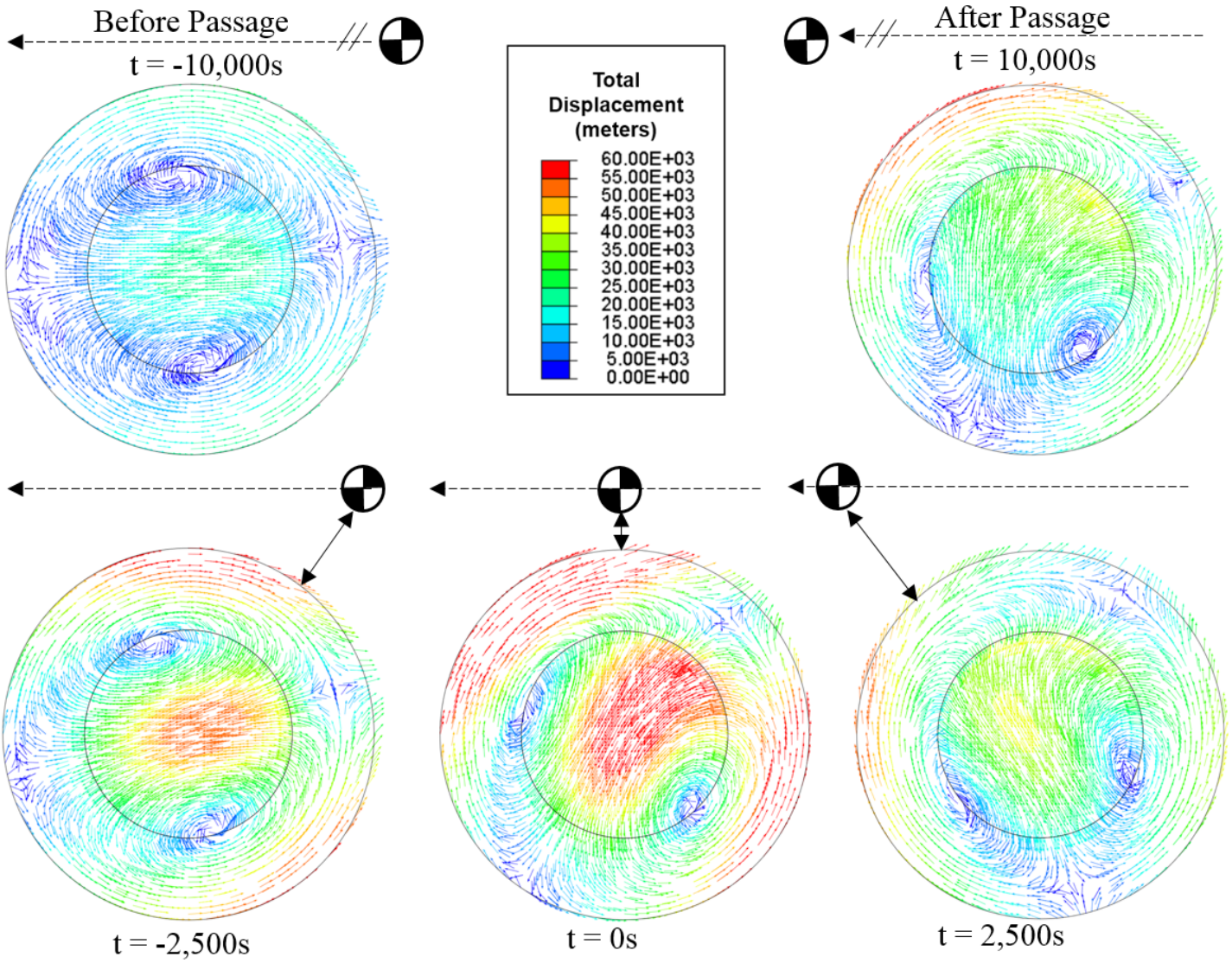

Figure 14. Cross sectional view of the stationary body (model Earth) along the equatorial x-y plane showing the total displacement for both mantle and core material occurring during the fly-by of an Earth mass object. Counter clockwise from the upper left are shown displacements at time steps referenced to time of nearest passage. The position of the fly-by mass is shown as it passes above the stationary object from right to left (indicated by arrows). Note the largest residual displacements after passage follow nearly parallel to the surface, approximately 60 km lateral displacement.

rates on the Moon and planets during the late heavy bombardment. *Astronomy and Astrophysics* 598: A67.

Sherburn, J.A., J.R. Baumgardner, and M.F. Horstemeyer. 2013. New material model reveals inherent tendency in mantle minerals for runaway mantle dynamics. In *Proceedings of the Seventh International Conference on Creationism*, ed. M.F. Horstemeyer. Pittsburgh, Pennsylvania: Creation Science Fellowship.

Sherburn, J.A., M.F. Horstemeyer, D.J. Bammann, and J.R. Baumgardner. 2011. Application of the Bammann inelasticity internal state variable constitutive model to geological materials. *Geophysical Journal International* 184:1023–1036.

Spencer, W.R. 1998. Geophysical effects of Impacts during the Genesis Flood. In *Proceedings of the Fifth International Conference on Creationism*, ed. R.E. Walsh., pp. 567-579. Pittsburgh, PA: Creation Science Fellowship.

Tsiganis, K., R. Gomes, A. Morbidelli, and H.F. Levison. 2005. Origin of the orbital architecture of the giant planets of the Solar System. *Nature* 435: 459–461.

Wiechert, U., A.N. Halliday, D.C. Lee, G.A. Snyder, L.A. Taylor, and D. Rumble. 2001. Oxygen isotopes and the Moon-forming giant impact. *Science* 294, no. 5541: 345-348.

Wise, K.P., S.A. Austin, J.R. Baumgardner, D.R. Humphreys, A.A. Snelling, and L. Vardiman. 1994. Catastrophic late tectonics: A global Flood model of earth history. In *Proceedings of the Third International Conference on Creationism*, ed. R.E. Walsh, pp. 609-621. Pittsburgh, Pennsylvania: Creation Science Fellowship.

Zhang, J., N. Dauphas, A.M. Davis, I. Leya, and A. Fedkin. 2012. The proto-Earth as a significant source of lunar material. *Nature Geoscience* 5: 251-255.

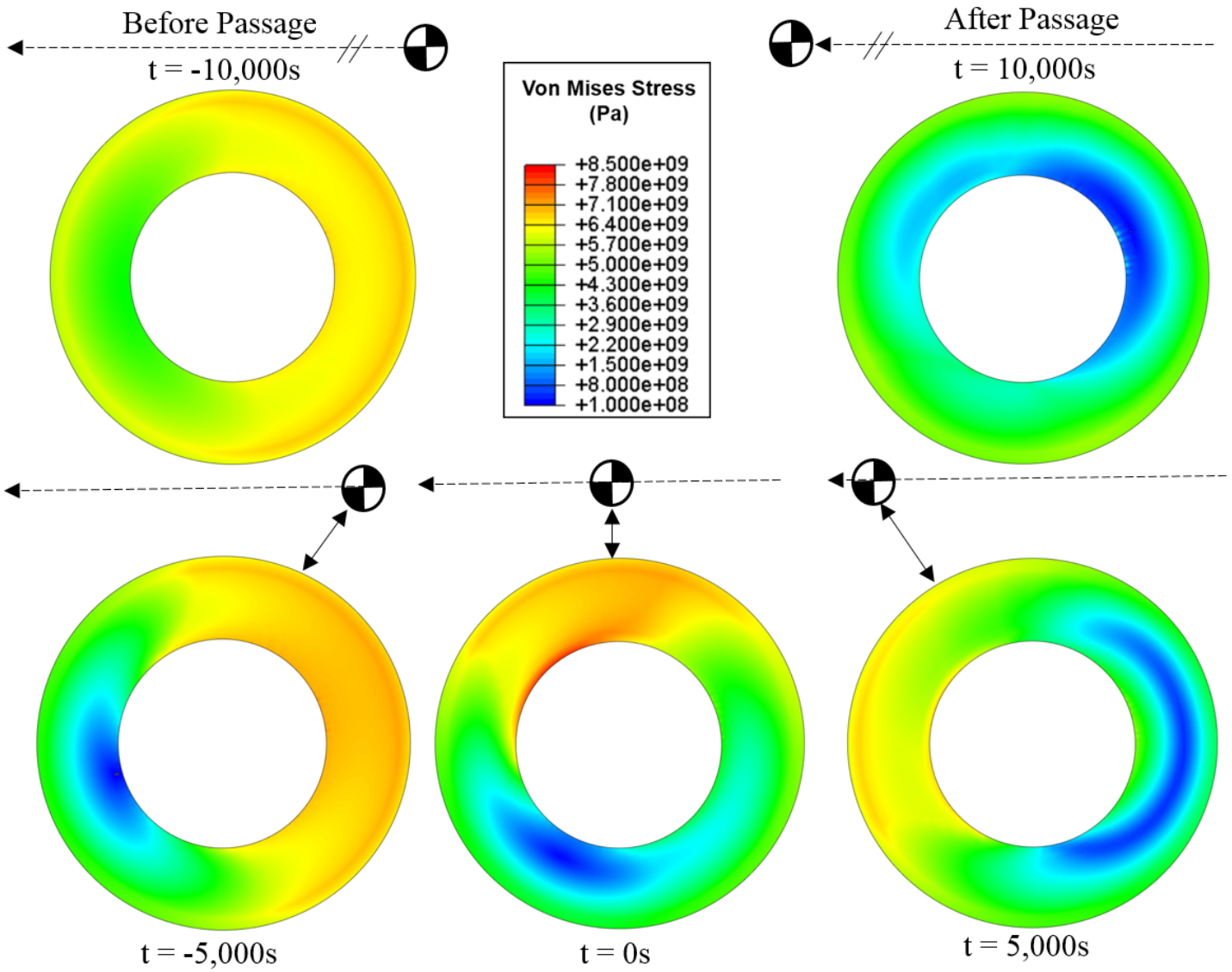

Figure 15. Von Mises stress contour for cross sections of the stationary body (model Earth) along the equatorial x-y plane for the near passage of an Earth mass object. Initial Von Mises stresses for simulation this step are carried forward from the preceding self-loading step. Counter clockwise from the upper left are shown Von Mises stress contours at time steps referenced to time of nearest passage. The position of the fly-by mass is shown as it passes above the stationary object from right to left (indicated by arrows). The highest value of mantle stress at the core mantle interface in the quadrant between the near-side and retreat faces. The band of reduced stress begins on the opposite side from the passing object and sweeps around to the approach face.

THE AUTHORS

Denver Seely studied electrical and mechanical engineering at Cedarville University earning a B.S.E.E. in 1999. He earned a M.S. degree in bioengineering from the University of Toledo in 2000. Denver studied astro/geophysics at the Institute for Creation Research graduate school (2005) and worked as facilities engineer at the AiG Creation Museum (2006-2008). He earned a Ph.D. in mechanical engineering at Mississippi State University (2018) researching metal layered composites and functionally graded materials using laser based 3D metal printing systems.

Andrew Bowman studied biology and engineering at Mississippi State University earning his B.A. in biological sciences in 2012 and his B.A. in mechanical engineering in 2014. Currently, he is a Ph.D. student in Mechanical Engineering at Mississippi State University conducting research in the area of multiscale modeling and computational engineering of viscoelastic materials.

Noah Cho is currently a Ph.D. student in computational engineering at Mississippi State University, with an emphasis on computational geophysics. His dissertation research involves development of improved numerical models for the deformation behavior of mantle, combined with an exploration of how that deformation behavior influences the earth's dynamics. The goal of his work is to model the plate tectonics during the Genesis Flood in a more realistic manner than ever before and to gain deeper insight into the physical processes that occurred during this cataclysm.

Mark Horstemeyer is a fellow of four societies (ASME, ASM, SAE, and AAAS), is a member of the European Union Academy of Sciences and has garnered international acclaim as he has published over 500 journal articles, conference papers, books, and technical reports with a citation impact h-factor of 52; he has given 150 lectures throughout the world (was named as honorary professor of Xihua University, Chengdu, China); and has won many awards (R&D 100 Award, AFS Best Paper Award, Sandia Award for Excellence, Ralph E. Powe Research Award, Ohio State's Thomas

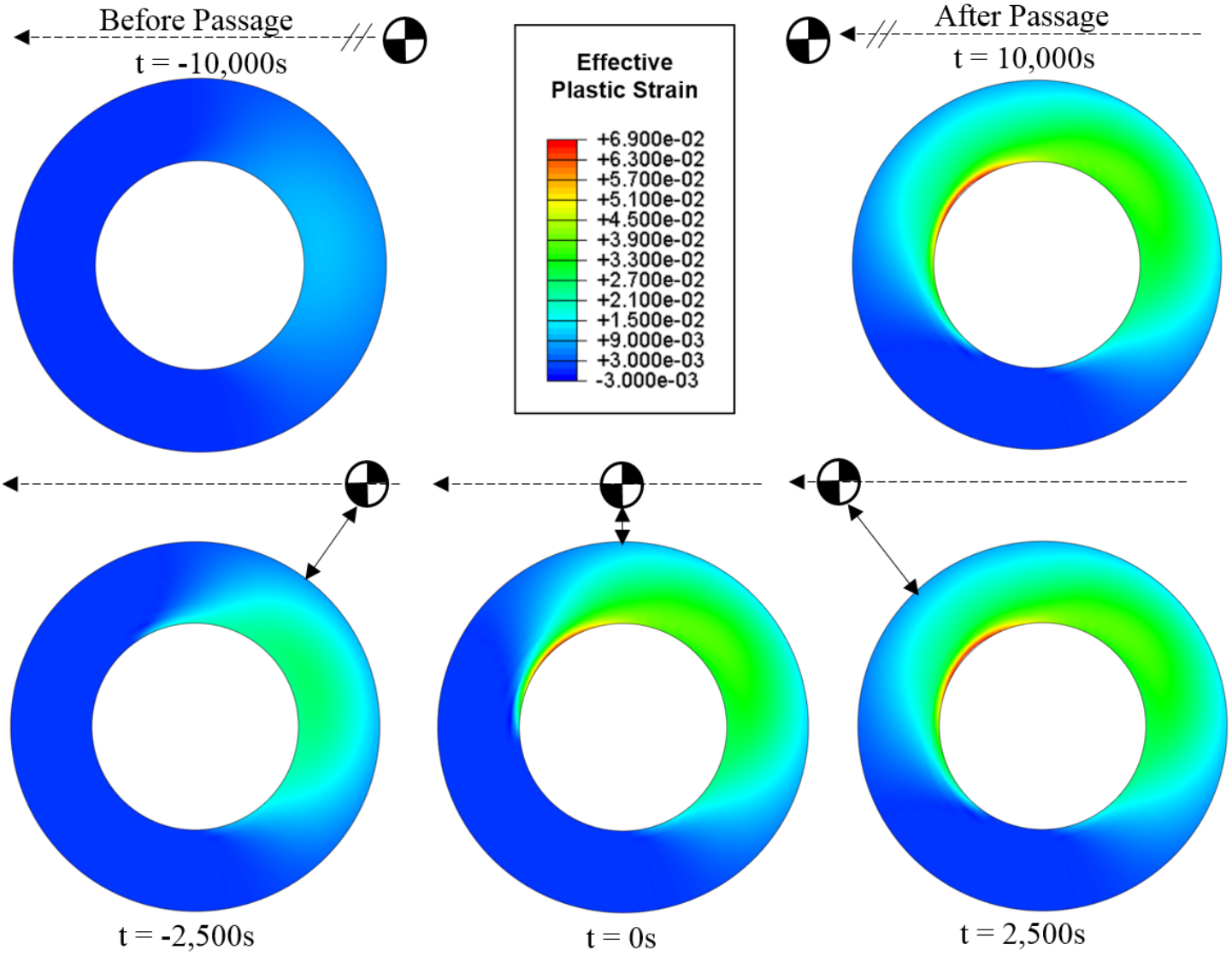

Figure 16. Equivalent plastic strain for cross sections of the stationary body (model Earth) along the equatorial x-y plane calculated from the internal state variable elastic-plastic model used for the mantle material during the fly-by of an Earth mass object. Counter clockwise from the upper left are shown total plastic strain at time steps referenced to time of nearest passage. All plastic strains were reset to zero at beginning of the simulation step (-10,000 seconds). Note the strong localization of plastic strain stress at the core mantle interface in the quadrant between the near-side and retreat faces.

French Alumni Achievement Award); and has mentored over 120 graduate students and post-doctoral researchers.

APPENDIX

Formulations for Self-Gravity and Passing-Body Forces

The following sections describes the ABAQUS implementation of the self-gravity force and the fly-by interaction force experienced by the stationary object during a near pass event. Although the calculation of the body force is relatively simple, the complexity of the formulations arises from tracking the distance between the fly-by object and each element within the stationary body. The use of a two-layer model (core/mantle) for the stationary body adds additional complexity as the gravitational potential is non-uniform throughout the body.

The force experienced within the core by each element (F_i) at a given distance from the origin (r_i) due to self-gravity is found using Newton's second law of motion:

$$F_i = M_i g \quad (1)$$

where M is the total mass of the element and g is the acceleration due to gravity given as:

$$g = \frac{M_c G}{r_i^2} \quad (2)$$

where M_c is the mass of the core material, r_i is the distance of the element from the origin, and G is the universal gravitational constant. Substituting $M_c = \rho_c V_c$, where ρ_c and V_c is the density and volume of a sphere with a radius r_i, into Equation 1 and simplifying, gives the final expression for the self-gravity on every element within the core as a body force:

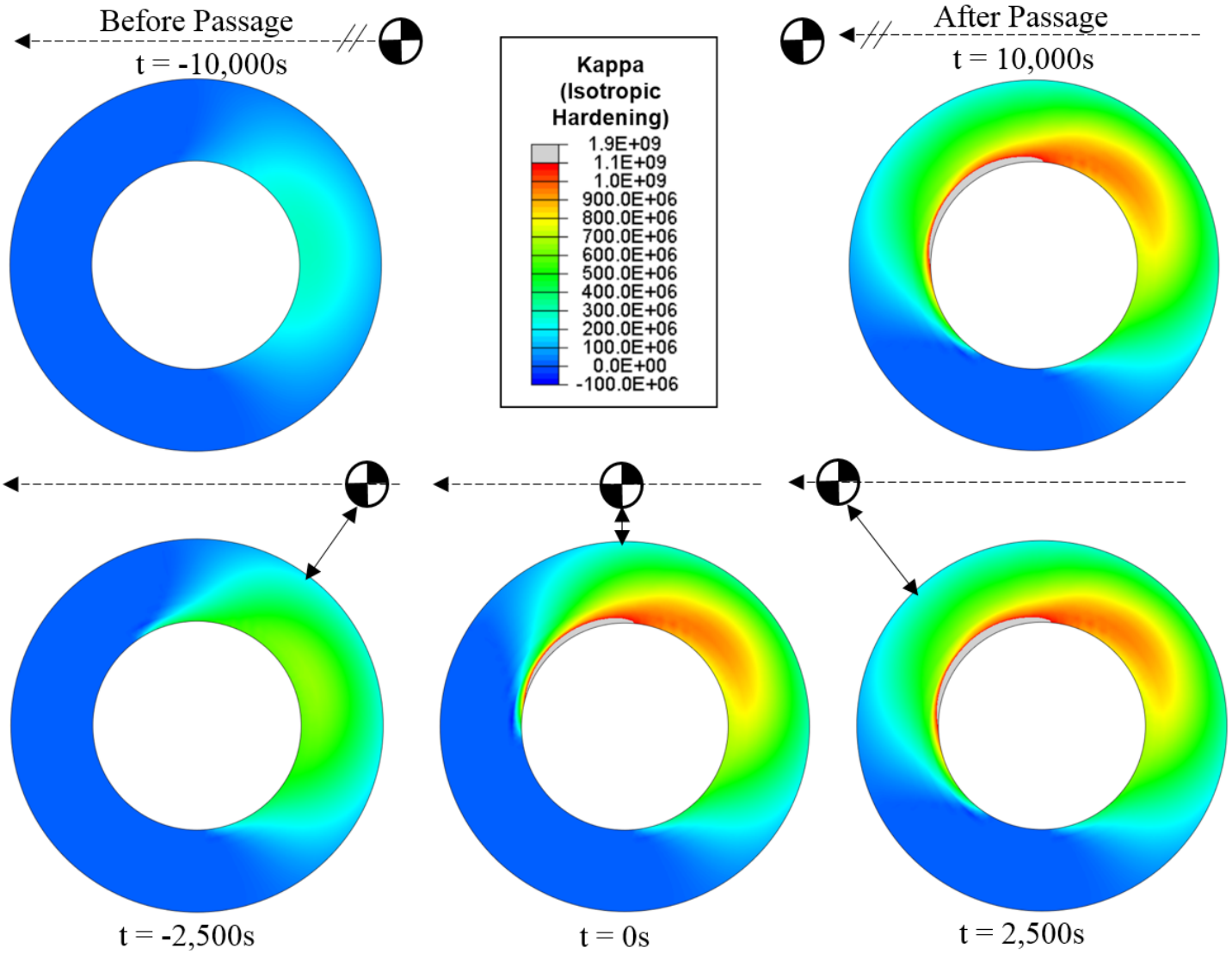

Figure 17. Isotropic hardening (kappa or SDV7) for cross sections of the stationary body (model Earth) along the equatorial x-y plane calculated from the internal state variable elastic-plastic model used for the mantle material during the fly-by of an Earth mass object. Counter clockwise from the upper left are shown isotropic hardening at time steps referenced to time of nearest passage. The pattern is not symmetric about the plane of nearest passage, but matches closely with the equivalent plastic strain.

$$\frac{F_i}{V_i} = \frac{4}{3}\pi G \rho_i^2 r_i \quad . \tag{3}$$

where V_i and ρ_i are the volume and density of a given element, respectively. Similarly, the self-gravity body force within each element of the mantle is also given by Equation 1, except the gravitational pull on each element has a contribution from the core material and mantle material, usually consisting of different materials with different densities, and changes the gravitational expression:

$$g = \frac{\left(M_{core} + M_{mantle}\right)G}{r_i^2} \quad . \tag{4}$$

Again, substituting M = ρV for the core and mantle, we have:

$$g = \frac{\frac{4}{3}\pi\left[\rho_{core} r_{core}^3 + \rho_{mantle}\left(r_i^3 - r_{core}^3\right)\right]G}{r_i^2} \quad . \tag{5}$$

Substituting the above expression into Equation 1 and simplifying gives the final expression for the self-gravity for each element within the mantle as a body force:

$$\frac{F_i}{V_i} = \rho_{mantle}\frac{\frac{4}{3}\pi\left[\rho_{core} r_{core}^3 + \rho_{mantle}\left(r_i^3 - r_{core}^3\right)\right]G}{r_i^2} \quad . \tag{6}$$

Finally, the force as a function of time on each element (F_j) induced during the near pass of the fly-by object is again found by Newton's second law as:

$$F_j(t) = \frac{GM_1M_2}{r_j(t)^2} \quad , \tag{7}$$

where M_1 is the mass of the stationary object, M_2 is the mass of the passing object, and $r_j(t)$ is the distance between the stationary and passing object's center of mass at specific times during the fly-by. Again, substituting M = ρV into the above expression for the stationary body gives the final expression for the body force experienced in each element as a function of time during the near

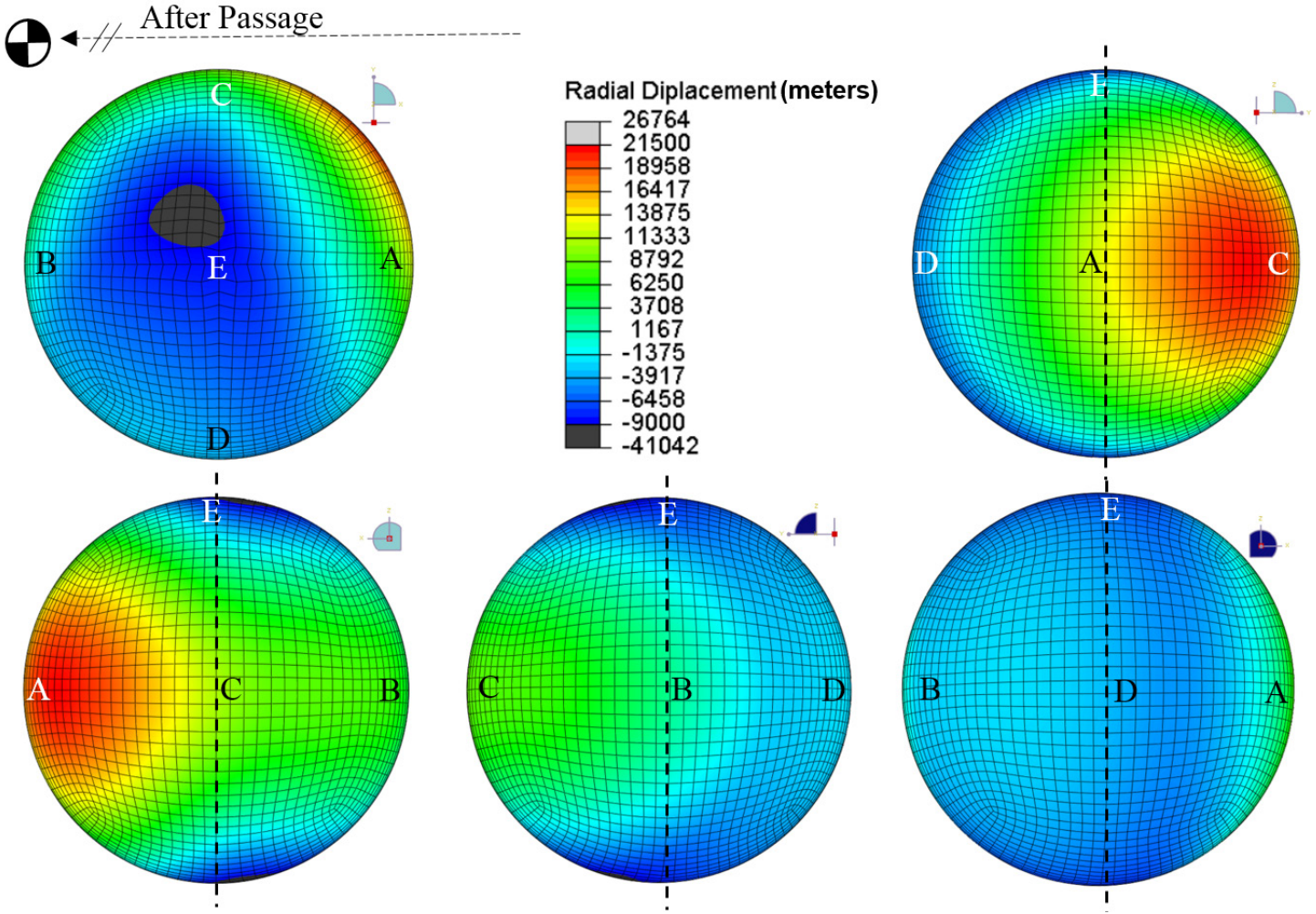

Figure 18. Surface view of the stationary body (two-layer model Earth) showing the permanent radial displacements (in meters) remaining after the fly-by of an earth mass object traveling at 20 km/sec at a peri-apsis distance of 45,000 km. The color coding indicating permanent topographical change after subsidence of the transient elastic displacements caused by the passage of an Earth mass object. Counter clockwise from the upper left are shown: (E) polar view, equatorial views of (C) near-side surface, (B) retreat-side surface, (D) far-side surface, and (B) approach-side surface. The value of the displacement is relative to the original surface as measured from the geometric center of the body. Note the global pattern of highlands (greens through red) and lowlands (blues).

pass event:

$$\frac{F_j(t)}{V_j} = \frac{G\rho_1 M_2}{r_j(t)^2}, \quad (8)$$

where ρ_1 is the average density of the stationary body found by averaging the densities of the core and mantle materials. The total force (F_t) experienced by each element on the stationary body during the fly-by is the sum of the self-gravity and passing body forces.

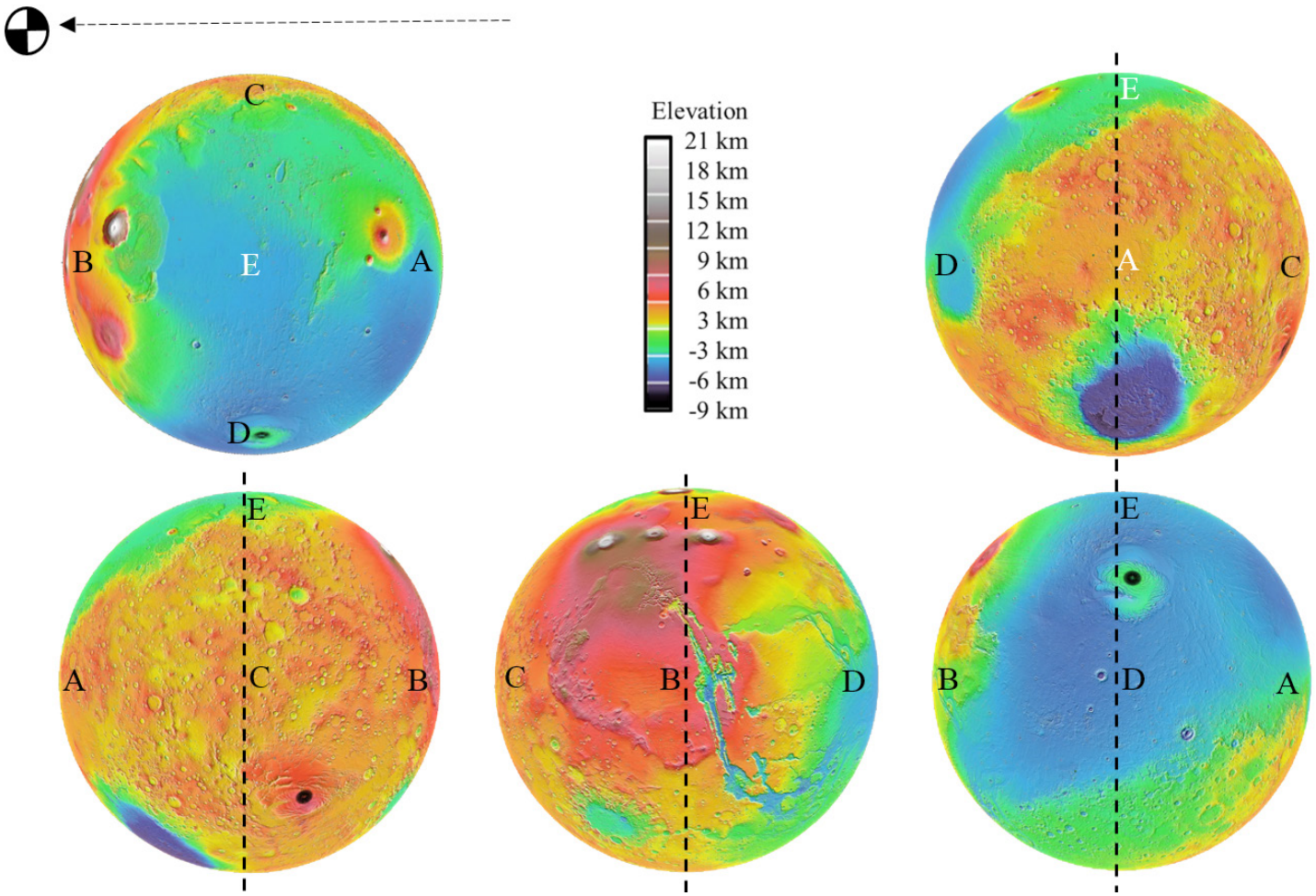

Figure 19. Topographical surface map of the planet Mars (NASA/JPL) projected onto a spherical surface. The global distribution of highlands and lowlands is consistent with the residual radial displacements observed in this study. Counter clockwise from the upper left are shown: (E) polar view, equatorial views of (C) near-side surface, (B) retreat-side surface, (D) far-side surface, and (B) approach-side surface. The polar and equatorial views refer to the axis of near passage which is offset from Martian rotation axis by approximately 50 degrees.